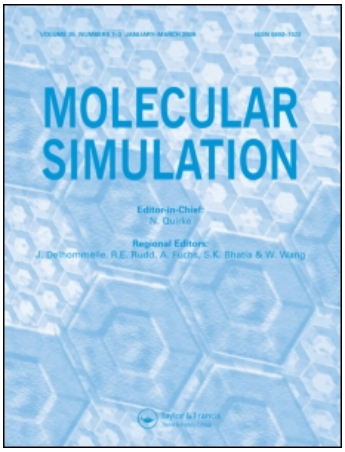

Molecular Simulation
Publication details, including instructions for authors and subscription information:
http://www.informaworld.com/smpp/title~content=t713644482

Capillary Condensation: A Molecular Simulation Study

J. P. R. B. Walton[a]; N. Quirke[a]
[a] BP Research International, Sunbury Research Centre, Middlesex, U.K.

To cite this Article Walton, J. P. R. B. and Quirke, N.(1989) 'Capillary Condensation: A Molecular Simulation Study', Molecular Simulation, 2: 4, 361 — 391
To link to this Article: DOI: 10.1080/08927028908034611
URL: http://dx.doi.org/10.1080/08927028908034611

Molecular Simulation, 1989, Vol. 2, pp. 361–391
Reprints available directly from the publisher
Photocopying permitted by license only

CAPILLARY CONDENSATION: A MOLECULAR SIMULATION STUDY

J.P.R.B. WALTON and N. QUIRKE

BP Research International, Sunbury Research Centre, Chertsey Road, Sunbury-on-Thames, Middlesex TW16 7LN, U.K.

(*Received July, 1988*)

The capillary condensation of a Lennard-Jones fluid confined to an adsorbing slit-like pore is studied using the grand canonical Monte Carlo method of molecular simulation for several values of the slit width, H. For each slit, we calculate the adsorbate density within the slit as a function of the chemical potential, or pressure, P, of the fluid – that is, the adsorption isotherm. Capillary condensation is the jump in density from a low, vapour-like value to a high, liquid-like value at some undersaturation $P/P^0 < 1$ (where P^0 is the saturation pressure). For large H, the transition is associated with metastable states and the system grand potential must be calculated to identify the point at which the two states are in equilibrium. As H is made smaller, the point of transition shifts to lower undersaturations while the metastable region shrinks and disappears at a critical width H_C. For $H < H_C$, the isotherms are continuous and exhibit steep (but not infinitely steep) risers connecting branches of low and high density. The length of the low density branch (i.e. the pressure at which the pore is completely filled) goes to – essentially – zero when the pore can accommodate just two adsorbed layers.

Consideration of the structure of the adsorbed phase reveals that the density jump at capillary condensation is localised to the central part of the pore space. The density of the layers that build up at the walls is insensitive to whether the overall density is vapour or liquid-like. The breakdown of the predictions of the Kelvin equation for the capillary condensation pressure is illustrated with reference to the simulation results.

KEY WORDS: Capillary condensation, grand canonical Monte Carlo, slit pores, Kelvin equation

1. INTRODUCTION

A bulk fluid at a temperature which is below that of its vapour-liquid critical point will undergo a phase transition from vapour to liquid as its chemical potential or pressure is raised past the saturation value at that temperature. A fluid which is confined (to, for example, the pores of a solid) by adsorbing walls will, in general, condense before this point is reached. This phenomenon, called capillary condensation, is usually invoked in the explanation of experimental adsorption isotherms which display the amount of fluid adsorbed by a porous solid as a function of fluid pressure P (or, more conventionally, the undersaturation P/P^0, which is the ratio of P to the saturation pressure at the temperature in question) [1]. Whilst these isotherms are sometimes reversible, so that the same path is followed on adsorption and desorption, they often exhibit hysteresis loops with adsorption occuring at higher pressures than desorption.

An example of a sorption isotherm which features hysteresis is displayed in Figure 1. As the pressure of the adsorbing vapour is raised from zero, there is a gradual increase in the amount adsorbed until at some undersaturation (around region A on the figure) a sharp rise occurs. This is associated with the (capillary) condensation of the vapour in the pores. All pores are filled with liquid at point B, and the remainder

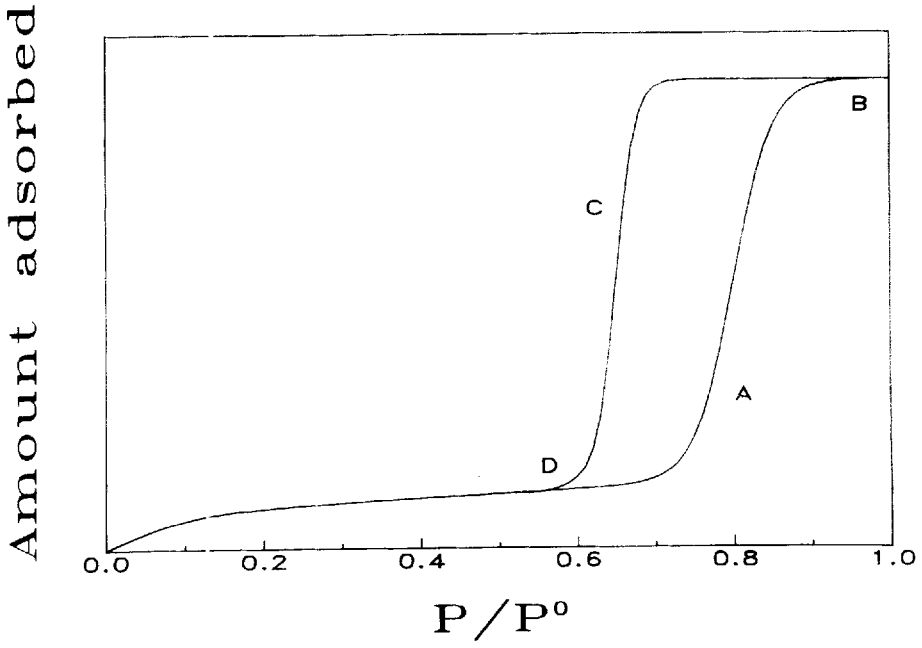

Figure 1 A schematic experimental adsorption isotherm for a typical mesoporous solid. Note the hysteresis loop ABCD, which is associated with capillary condensation. Isotherms of this type are often referred to [1] as type IV.

of the isotherm is flat. Upon reduction of the pressure from its saturation value, the liquid phase in the pores can persist to a lower pressure than that at which the transition to liquid occurred on the adsorption branch; a sharp drop in the amount adsorbed is observed around region C, where capillary evaporation of the liquid takes place. All pores are filled with vapour at point D, and the remainder of the desorption branch closely follows the adsorption part of the curve. The adsorption - desorption hysteresis loop ABCD is a signature of capillary condensation. By contrast, Figure 2 shows an isotherm which does not display hysteresis; the amount adsorbed rises sharply at low pressures and flattens out to a constant value.

The form of the sorption isotherm has been of practical significance for a long time because of the possibility of using it to infer details about the structure of the adsorbent. Unfortunately, the extraction of this information is usually very difficult, chiefly because of a poor understanding of the mechanisms involved in the phase changes which can occur inside a pore. Traditionally, a distinction has invariably been made between adsorption processes in *mesopores* and in *micropores* [1]. The former (defined, somewhat arbitrarily, as having sizes between 20 and 200 Å) are believed to exhibit capillary condensation during adsorption, while the latter (smaller than 20 Å) are said to fill reversibly as the fluid pressure is increased, a process known as micropore filling. Thus, Figure 1 would be characteristic of a sorbent which is primarily composed of mesopores, while Figure 2 is typical of a microporous adsorbent. This dichotomy between adsorption mechanisms causes inconsistencies in the analysis of isotherms obtained from adsorbents containing both types of pore and it

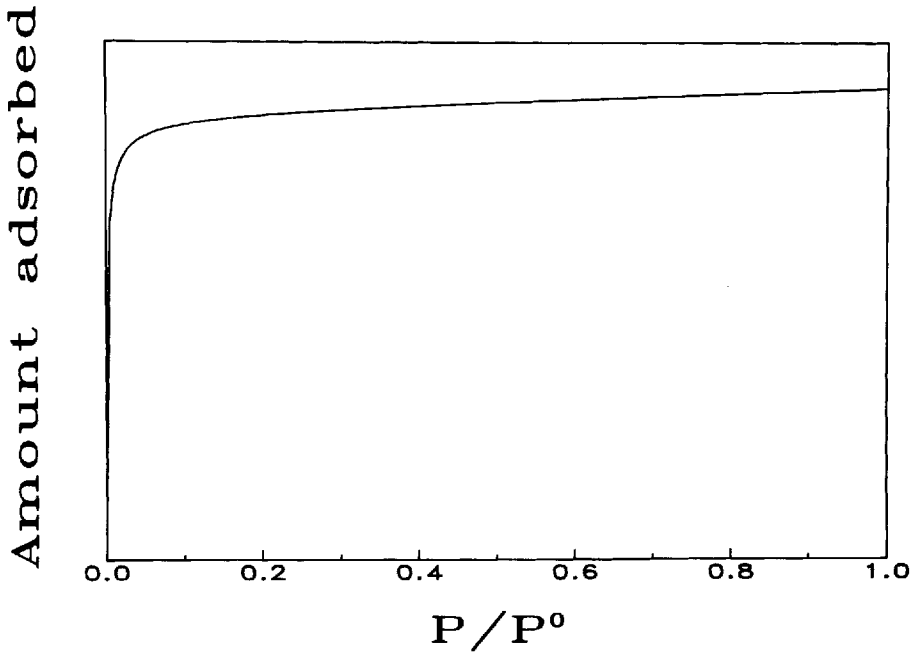

Figure 2 Schematic experimental adsorption isotherm for a predominantly microporous solid. This type of isotherm is often referred to as type I [1].

appears that more information is needed about what happens to capillary condensation as the pore size becomes small. In this paper we use molecular simulation to address this problem, studying the phase equilibria and structure of the adsorbed phase inside a model pore with especial reference to its dependence on pore size. A few results from the preliminary stages of this work have already appeared elsewhere [2].

Several workers have made previous theoretical studies of pore-fluid systems. Particular emphasis has been placed on confinement within a single, isolated idealised pore such as a slit (two flat parallel walls of infinite area) or a cylinder (an infinitely long cylindrical hole in a structureless solid). Such studies (of which the present paper is one) choose to ignore the effects of surface non-uniformity, size variations and connectivity which are present in the pores of a real adsorbent. Some of this previous work has been done using molecular simulation [3–11,22], but most of it has involved a simplified molecular model for the fluid [11–22]. Thus, Lane and Spurling [3], van Megen and Snook [4], and Hawley *et al.* [5] have all observed capillary condensation in their grand canonical simulations of a Lennard-Jones fluid in slits. Similar results have been recently obtained for cylinders by Peterson *et al.* [6–8,11], Heffelfinger *et al.* [9] and Panagiotopoulos [10].

More extensive results have come from simplified model approaches such as density functional theory [11,16–22] or an equivalent mean-field theory [12–15] which have revealed an intriguing richness of phase behaviour resulting from the interplay between capillary and wetting effects in these systems. In particular, it has been shown [18,19] that the shape of the adsorption isotherm is qualitatively dependent on

whether or not the temperature (T) is in excess of T_W, the so-called wetting temperature, at which a transition from *partial* to *complete* wetting of a single wall by the fluid occurs [24]. For $T \geqslant T_W$ (complete wetting), the angle of contact between the liquid inside the pore and the pore wall is zero and wetting films develop on the walls as saturation is approached, which makes the vapour branch of the isotherm much steeper than when the fluid partially wets the pore walls ($T < T_W$). This in turn has implications [18,19] for thermodynamic treatments of these systems involving (for example) the Kelvin equation [1,17] which gives the pressure at which capillary condensation occurs in terms of the pore size and the properties of the infinite or semi-infinite fluid. The appearance of wetting films above T_W decreases the effective pore size (in a manner which depends on the form of the solid-fluid potential [17]) which causes the transition pressure to be much smaller than the Kelvin prediction, even for rather large pores. If the thermodynamic equations are self-consistently modified [17] to allow for the wetting films the discrepancy is reduced. For $T < T_W$, the Kelvin equation remains accurate down to smaller pore sizes [18,19].

In density functional theory, the effect of the repulsive part of the intermolecular potential is usually modelled using a local approximation which neglects short-ranged correlations. Thus, the theory does not correctly predict the oscillatory fluid structure induced by packing against an impenetrable wall, an omission which may be expected to have rather serious consequences when the pore size becomes small. The present authors [22] have checked the performance of the theory against simulation for a supercritical fluid in a series of slits and have shown that it underestimates the overall density of the adsorbed phase, especially for slit widths H which are smaller than about five molecular diameters. Tarazona *et al.* [23] have compared results obtained from the theory with those given by a more sophisticated version [25] which uses a non-local approximation for the repulsive forces. They discovered that the inclusion of short-ranged correlations decreases the wetting temperature and shifts the capillary coexistence curve to smaller H. Moreover, the local theory becomes unrealistic in the limit of very small slits since it does not predict two-dimensional (2D) phase equilibria. The coexistence curve of the non-local theory, by contrast, shows a crossover to 2D liquid-vapour coexistence for sufficiently small H at temperatures $T < T_C^{(2)}$, the 2D critical temperature. For $T > T_C^{(2)}$, (and for all T in the local theory) the coexistence isotherm ends in a capillary critical point (H_C, P_C) [14–16,18,19] with no capillary condensation for $H < H_C(T)$ or $P < P_C(T)$. More recently, Peterson *et al.* [11] have compared the predictions of both types of density functional theory to those of simulation for fluid in the cylindrical pore.

Our paper is arranged as follows. In the following section we discuss our models for the fluid and the pore and determine (§2.2) the location of our simulation with respect to (a) $T_C^{(2)}$ and (b) T_W for the system studied here. Section 3 contains a description of the simulation method and the way in which the metastable states encountered in some of the runs in the larger slits may be identified through the calculation of the grand potential Ω. We describe two expressions for Ω, and compare results obtained using both of them in one of the simulation runs. The full set of simulated results are presented in Section 4 for the adsorption isotherms (§4.1) and density profiles (§4.2) and are summarised in Section 5.1, paying particular attention to the way in which the phase behaviour of the fluid is altered as it becomes increasingly confined. In §5.2, the metastable states are discussed and their possible relationship with hysteresis effects in experimental adsorption isotherms is explored. The break-

down of the thermodynamic description of capillary condensation is illustrated in §5.3. We conclude (§6) with some final remarks.

2. THE PORE-FLUID MODEL

In this section, we describe our model for the pore, our representation of the fluid within the pore and the way in which it interacts with the solid material comprising the walls of the pore. The position of the temperature of the simulation with respect to $T_C^{(2)}$ and T_W is estimated, and the implications this has for the sorption behaviour of our system are outlined.

2.1 Interaction potentials

We study the fluid whose interactions are those of the cutoff and shifted Lennard-Jones (LJ) potential,

$$\begin{aligned} u(r) &= u_{LJ}(r) - u_{LJ}(r_C), \qquad r \leqslant r_C \\ &= 0, \qquad r > r_C \end{aligned} \tag{1}$$

where

$$\begin{aligned} u_{LJ}(r) &= 4\varepsilon_{ff}[(\sigma_{ff}/r)^{12} - (\sigma_{ff}/r)^6], \\ r_C &= 2.5\sigma_{ff}, \end{aligned} \tag{2}$$

and, as usual, appropriate combinations of the parameters σ_{ff} and ε_{ff} are used to reduce the properties of the system into a dimensionless format, e.g. $H^* \equiv H/\sigma_{ff}$, $\rho^* \equiv \rho\sigma_{ff}^3$, $\mu^* \equiv \mu/\varepsilon_{ff}$ and $T^* \equiv k_B T/\varepsilon_{ff}$, where k_B is Boltzmann's constant. The bulk thermodynamic properties of this fluid may be derived from the equation of state of the full LJ fluid [26] by calculating the usual correction terms for the effect of the missing part of the potential. Thus, for example, we may convert the chemical potential μ of the fluid to the undersaturation, since it is usually more meaningful to present the results (e.g. the adsorption isotherm – see §1) in terms of this variable. The equation of state is known to be quite accurate at the temperature at which we are working; its prediction for the saturation pressure of the full LJ fluid, for example, is within a few percent of a more direct estimate obtained via grand canonical Monte Carlo [27]. We emphasise that all properties calculated in the pore-fluid simulation are for the fluid with the finite ranged potential $u(r)$ and, in particular, that we do not attempt to predict the properties of the fluid interacting via the non-truncated potential inside the pore, which would involve calculating the correction terms for the inhomogeneous system [28].

The fluid is contained within a slit-like pore formed (see Figure 3) from two planes of solid that are infinite in area and separated by a distance H. The pore-fluid potential may be calculated [29] by (a) assuming the solid (of density ρ_s) to consist of an infinite set of continuous lattice planes of spacing Δ, (b) assuming an LJ potential to exist between each fluid molecule and each volume element in the solid and (c) integrating this potential over the solid. We obtain

$$\begin{aligned} v(z) &= v_1(z) + v_1(H-z), \quad 0 < z < H, \\ &= \infty, \qquad \text{otherwise}, \end{aligned} \tag{3}$$

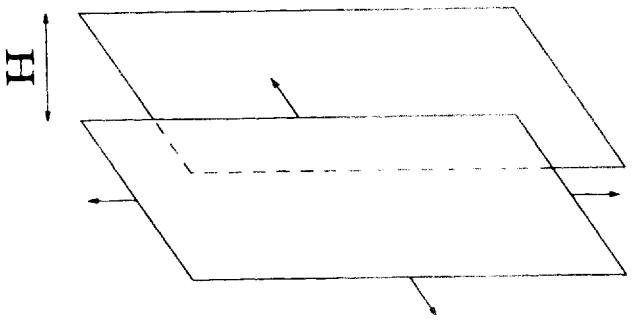

Figure 3 Sketch of the model for the slit-like pore used in this work. Two planes of solid are separated by a distance H. The planes are infinite in area and the solid extends (on each side of the slit) for an infinite distance in the direction normal to the plane.

where [29]

$$v_1(z) = 2\pi\varepsilon_{sf}\sigma_{sf}^2\rho_s\Delta[2/5(\sigma_{sf}/z)^{10} - (\sigma_{sf}/z)^4 - \sigma_{sf}^4/3\Delta(z + 0.61\Delta)^3]. \quad (4)$$

We note in passing that the presence of the repulsive component of $v_1(z)$ causes the two-dimensional limit of these slits to occur at a *finite* value of H (see below), in contrast to slits using (for example) the less realistic integrated Yukawa form for $V_1(z)$ [16–19,23] whose two-dimensional limit is at $H = 0$.

In this paper, we use the parameter values [29,30]

$$\varepsilon_{ff}/k_B = 95.2\,\text{K}, \sigma_{ff} = 3.75\,\text{Å}, \varepsilon_{sf}/k_B = 51.6\,\text{K}, \sigma_{sf} = 3.57\,\text{Å},$$

and

$$\rho_s = 0.114\,\text{Å}^{-3}, \Delta = 3.35\,\text{Å}$$

These could be considered to be appropriate to fluid nitrogen and solid graphite. Our simplified representation of the N_2 molecule omits its shape and charge distribution. Given the rather high reduced temperature of this study (see §2.2), the qualitative features of the results presented here are unlikely to be sensitive to the fine details of the intermolecular potentials, although we expect molecular shape to influence the way in which the adsorbate packs into very small slits and the thickness of the wetting layers in larger slits will be rather sensitive to the balance between the fluid-fluid and solid-fluid forces (we return to this latter point below – see §6).

Figure 4 shows the reduced pore-fluid potential $v^*(z^*)$ for several values of H^*. The size of its minima only depends on H^* when H^* becomes small and the two minima coalesce at $H^* = 2.152$, which we may somewhat arbitrarily associate with the onset of 2D-like behaviour in these slits. We note that this potential is, for large H^*, deeper (by a factor of roughly four) than that which would be appropriate for fluid argon in a slit of solid carbon dioxide – partly because of the semi-explicit description of the lattice planes in (4), and partly because of the comparatively high value of ρ_s for graphite. The Ar/CO_2 system has been extensively used by other theoreticians in this area [3,6–11,16,18–20]; by contrast, we have chosen to work with a model reminiscent of N_2 and graphite in an attempt to make future contact with the large body of experimental sorption measurements [1] which have been performed on graphites using N_2 as the adsorbate.

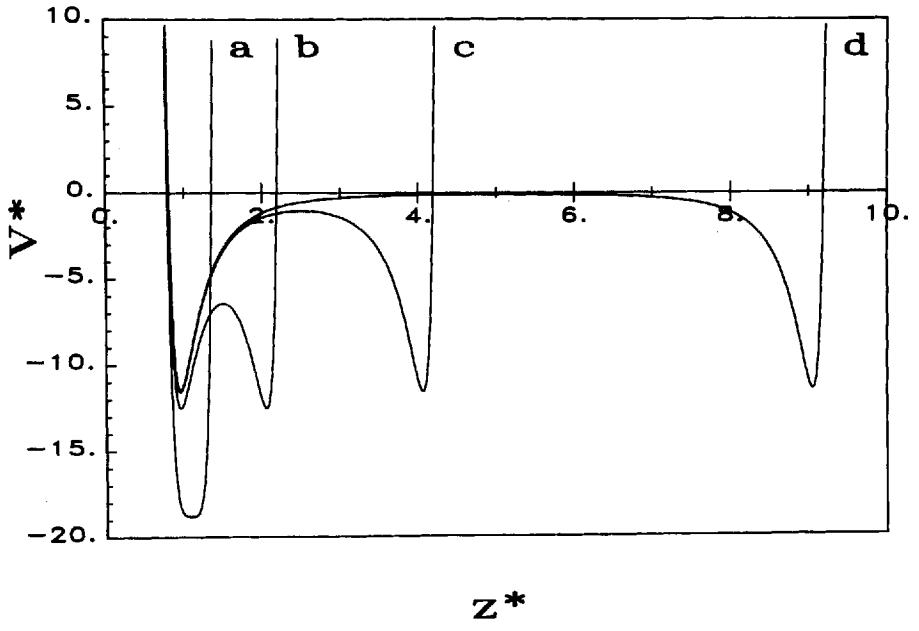

Figure 4 Reduced solid-fluid potentials $v^*(z^*)$ for nitrogen in graphite slits of reduced widths $H^* = 2.152$ (a), 3 (b), 5 (c) and 10 (d). $v^* \equiv v/\varepsilon_{ff}$, $z^* \equiv z/\sigma_{ff}$ and $H^* \equiv H/\sigma_{ff}$.

2.2 Some significant temperatures

The temperature of the present study was set at $T^* = 0.8$, or 0.71 $T_C^{(3)*}$ ($T_C^{(3)}$ the three dimensional critical temperature). This corresponds to an unreduced temperature of 76K, which is close to the boiling point of nitrogen at 1 atm, at which adsorption experiments are usually performed. As argued in §1, in making contact with previous theoretical work in this area, it is important to try to estimate where this is in relation to (a) $T_C^{(2)}$, the 2D critical temperature, and (b) the wetting temperature, T_W.

Several attempts have been made to calculate $T_C^{(2)*}$ for the LJ fluid [31,32]. Although this is not known with as much certainty as $T_C^{(3)}$, its value is probably less than 0.6. Reddy and O'Shea [31] have recently conflated the results of a large number of simulations into an equation of state for the 2D fluid which has $T_C^{(2)*} = 0.537$; other estimates via different methods are in reasonable agreement with this value [32]. Truncating the potential shifts T_C downwards (in three dimensions by about 17% for $r_C^* = 2.5$) and so we may be sure that our calculations are at a temperature which is in excess of $T_C^{(2)}$ for our fluid. Thus, for very narrow slits, we would not expect to encounter two-dimensional liquid-vapour coexistence.

Almost all the calculations of the wetting temperature have been performed for the Ar/CO_2 mentioned above. Much of this work has been done using both versions of the density functional theory referred to in §1. When the full LJ potential is used to model the fluid-fluid interactions, the local theory gives a value for the ratio $T_W/T_C^{(3)}$ of about 0.9 [33], while the more realistic non-local version predicts this to be roughly 0.6 [23,24]. The effect of truncating the fluid-fluid potential is rather unclear now, since it changes the tensions of the solid-vapour, solid-liquid and liquid-vapour

interfaces. T_W is determined by the balance between these three quantities and it has been shown [35] that it may be altered by changing the form or the relative range of $u(r)$ and $v(z)$. The cutoff and shifted LJ potential has been used by Heffelfinger *et al* [10] in their simulations of argon in cylinders of solid CO_2. They observe complete wetting of the cylinder walls at $T/T_C^{(3)} = 0.63$ for a reduced cylinder radius $R^* = 5$, but the wall-fluid potential for a cylinder is more attractive than for a planar wall (at which T_W is defined) and so it is possible that T_W for their system is larger than this temperature. However, we strongly suspect that, in comparing Ar/CO_2 to the system studied in this paper, the dominating feature is the enhanced depth of our wall-fluid potential (see §2.1), which will act to decrease T_W. Thus, given the temperature of our study, we may be reasonably confident that we are in the complete wetting regime, even though the actual value of T_W for our model N_2 on graphite is at present unknown.

3. THE SIMULATIONS

The adsorption process corresponds to a system of fixed volume in contact with a reservoir of adsorbate at fixed temperature and chemical potential. These are the variables of the grand canonical ensemble, and we have used Adams' grand canonical Monte Carlo method [36,37,27] to simulate adsorption in the system described in §2. This is similar to conventional (canonical) Monte Carlo, where molecular moves are given a Boltzmann chance (which depends on T) of occurring but, in addition, molecules are created and destroyed with a probability that is a function of both μ and T. In this method, it is well known [36–39] that the fraction of attempted creations and destructions that are successful falls off as the density approaches liquid-like values. In order to try and more thoroughly explore the range of possible values for N, the number of molecules, we have slightly modified the program so that each compound step in the simulation consists of n attempted creations, followed by one attempted move, followed by n attempted destructions. In the work presented here, n has been set equal to 10.

Each simulation run started with an equilibrium period of at least 5×10^4 compound steps after which calculation of the running averages was started. The total number of compound steps in each run was at least 5×10^5, and in some cases was as much as 1.5×10^6. The starting configuration for each run was either (a) taken from a different run (at a higher chemical potential) or (b) created by placing a single molecule at a random location in the system. These two ways of starting were used when checking for metastable states. For some values of H and μ, both a high density [started from (a)] and a low density [started from (b)] state were obtained and separately persisted for the duration of the runs. The limits of the metastable region for a slit of fixed H are μ_{min} and μ_{max}; for $\mu < \mu_{min}$, the run, if started from (a), would collapse to a low density state, while for $\mu > \mu_{max}$, the density of a run which started from (b) would jump to a high value. Figure 5 shows this happening for two runs at (roughly) μ_{min} and μ_{max} for the slit with $H^* = 10$. No further change occurred in either simulation over the remainder of the runs, which were each of 5×10^5 compound steps in length.

The reduced breadth of the simulation cell in the x and y directions was 10 in the majority of the work described here; some runs, however, were done with different values for this dimension to check on the size dependence of the results. As usual,

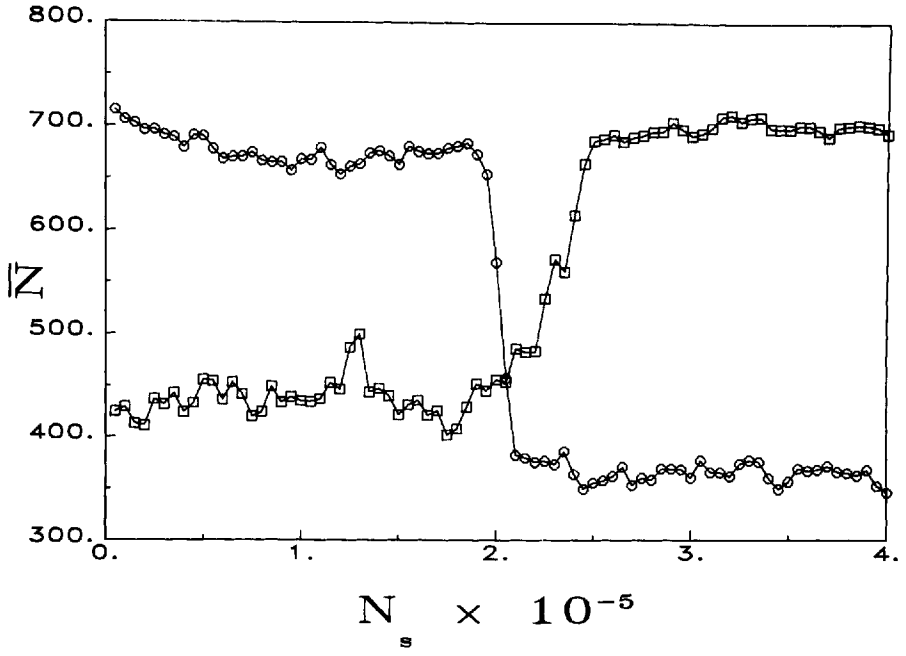

Figure 5 The limits of metastability in the $H^* = 10$ slit. $\bar{N}$ is the mean number of molecules in the slit (averaged over blocks of 5000 steps) and N_S is the number of steps in the run. Circles: $\mu^* = -4.041$ ($\equiv \mu^*_{min}$, see §3) corresponding to $P/P^0 = 0.4$; squares: $\mu^* = = -3.782$ ($\equiv \mu^*_{max}$) or $P/P^0 = 0.563$. Here, μ^* ($\equiv \mu/\varepsilon_{ff}$) is the reduced configurational chemical potential and P^0 the saturation pressure.

periodic boundary conditions were imposed in the x and y directions. Most of the runs were done with a reduced slit width H^* which was between 3 and 20, corresponding to a range of between about 11 and 75 Å, which straddles the division between the mesopore and micropore regimes (see §1). In addition, some runs were done with larger slits ($H^* = 40,60$) to study the adsorption behaviour of essentially isolated walls. It should be noted that all the slits studied in this paper had widths which were a whole number of molecular diameters in size. This facilitates the formation of layers in the adsorbed phase; in general we found (see §4.2) that a slit of reduced width H^* is filled by $H^* - 1$ layers for $H^* \lesssim 7$. An analogous (perhaps heightened) effect occurs in cylinders where the fluid packs in concentric annuli [6–11]. The way in which the structure in cylinders is affected by varying R^* through non-integral values has been investigated by Peterson and Gubbins [8] and (more extensively) by Panagiotopoulos [10] who found that the pronounced variations in local structure within the pore appeared to have little effect on the phase equilibria. However, using the non-local density functional theory, Tarazona *et al* [24] have found that packing effects at small H and low T ($\sim 0.5\ T_C^{(3)}$) produce oscillations in the coexistence curve for both slits and cylinders. Because of the rather high temperature at which we are working (see §2.2) we would not expect packing (or lack of it) to have a significant effect on the coexistence curve; indeed, we shall find (§4.1) that it terminates in a critical point at a slit width which is much greater than those at which oscillations have been observed.

During the simulation we calculated the density profile

$$\rho(z) = \langle N(z) \rangle / A\delta \tag{5}$$

where $\langle N(z) \rangle$ is the mean number of particles in the slice of width δ at z and A is the cross-sectional area of the simulation cell. For all the runs reported here, δ was set at $H/100$. The overall density of fluid in the slit is

$$\Theta = \frac{1}{H} \int_0^H \rho(z)\, dz = \langle N \rangle / AH \tag{6}$$

where $\langle N \rangle$ is the mean number of particles in the system. Θ is related to Γ, the adsorption excess by

$$\Gamma = \frac{1}{2} \int_0^H [\rho(z) - \rho_b]\, dz = \tfrac{1}{2} H(\Theta - \rho_b). \tag{7}$$

Here, ρ_b is the density of the bulk fluid at the same T and μ and a factor of $\frac{1}{2}$ has been included because we have two surfaces in the slit.

We also calculated the grand potential Ω which is the free energy appropriate to the grand canonical ensemble [40]. The determination of this is one (but not the only [9–11]) way to obtain the points of phase coexistence in the pore. In the bulk, $\Omega = -PV$, where P is the pressure and V the volume of the system. For a system which features a planar inhomogeneity, this may be generalised by considering the work done on a subsystem during the creation or destruction of part of it [41]. The result is

$$\Omega = -A \int_0^H P_T(z)\, dz \tag{8}$$

where $P_T(z)$ is the transverse component of the pressure tensor at z. It is now well-known that there are an infinity of choices for the set of intermolecular forces which contribute to $P_T(z)$ [42]; this leads to an arbitrariness in $P_T(z)$, as well as its first, second, etc. moments with respect to z [43,41]. Its zeroth moment (above) is, however, well-defined [41–43]. Microscopically, we have, for pairwise additive intermolecular forces

$$\Omega = -\langle N \rangle k_B T + \tfrac{1}{2} \left\langle \sum_{i>j} \sum (r_{ij}^2 - z_{ij}^2)/r_{ij}\, du/dr_{ij} \right\rangle. \tag{9}$$

Here, r_{ij} is the distance between molecules i and j and z_{ij} is the difference in their z coordinates.

Such a route to Ω (which may be termed *mechanical*) does not exist for a system having cylindrical symmetry, since the zeroth (as well as the first, etc.) moment of P_T is now arbitrary and it is not possible to give an unambiguous definition of Ω in terms of this quantity [44]. Instead, Peterson *et al* [8,11] have used a *thermodynamic* route to Ω which involves integration of the relations

$$\left(\frac{\partial \Omega}{\partial \mu}\right)_{T,H} = -\langle N \rangle \tag{10}$$

which gives the change in Ω between two points on an isotherm (at fixed H), and

$$\left(\frac{\partial(\Omega/T)}{\partial(1/T)}\right)_{\mu,H} = U - \langle N \rangle \mu \tag{11}$$

Table 1 Comparison of thermodynamic and mechanical routes to Ω.

$-\mu'^*$	P/P^0	$\langle N\rangle/A^*$	$-\Omega_T^*/A^*$	$-\Omega_M^*/A^*$
12	1.8×10^{-5}	0.14	0.088	0.101 (9)
10	2.2×10^{-4}	1.26	1.49	1.5 (2)
8	2.7×10^{-3}	1.50	4.30	3.9 (3)
6	0.033	1.78	7.57	5.6 (3)
3.92	0.47	3.98	12.6	9.9 (9)
3.78	0.56	4.45	13.6	10.5 (8)

Comparison of the two routes to Ω (see §3) at $T^* = 0.8$ for the slit of reduced width $H^* = 10$. Here, μ'^* is the reduced configurational chemical potential (that is, $\mu^* - 3T^* \ln\Lambda$, with Λ the de Broglie wavelength), P/P^0 the undersaturation and $\langle N\rangle/A^*$ the mean number of molecules in the slit per unit reduced cross-sectional area. Ω^*/A^* is the reduced grand potential per unit reduced area, calculated from the thermodynamic route (Ω_T) using (11), and the mechanical route (Ω_M) from (10). The figures in brackets are the estimated uncertainty in the last decimal place.

(here, U is the total internal energy) to give the variation in Ω between two points (at the same μ and H) on different isotherms. By integrating (10) up from low μ – where the fluid is ideal, and $\Omega(N)$ is known explicitly – Ω may be found anywhere on the isotherm, in the absence of a phase change (where N changes discontinuously with μ). Peterson *et al.* thus obtain Ω for a high density point on a high temperature (continuous) isotherm, and then use (11) to get Ω at a corresponding point at a lower temperature. This then yields the grand potential for the liquid branch of the low-temperature isotherm; Ω for the vapour branch can be calculated using (10). Since we have restricted ourselves to one temperature in this work, this method is not appropriate for the determination of the point of capillary coexistence here, but we may nonetheless obtain the vapour branch Ω from (10) and compare its values with those obtained via the mechanical route (9). Table 1 shows that, for the $H^* = 10$ slit, the overall agreement between the two routes is quite good, but seems to get somewhat worse as the end of the vapour branch (at $P/P^0 = 0.563$) is approached with the thermodynamic estimates being rather larger than the mechanical one. It is not clear whether this difference is significant, but the two routes appear to be at least qualitatively consistent with each other. For hard spheres within a slit formed from two hard walls, Henderson and van Swol [41] obtained good agreement between the thermodynamic and mechanical routes to the surface tension (which, for this geometry, is equivalent to determining Ω if the pressure in the bulk phase is known), but found the thermodynamic route to be the more accurate of the two. However, as noted above, the use of this route to Ω in the present study would require many more runs to be performed at higher temperatures for each pore. Although the mechanical route is probably less accurate (see, e.g. Figure 9, below) it does have the advantage of being a more direct means of access to Ω, and it is this route which has been followed in the work presented here.

4. RESULTS

4.1 Adsorption Isotherms

In this section, some of the results for the adsorption isotherms obtained from the simulations are presented. These are plots of Θ^*, the mean reduced density of fluid within the pore, versus the fluid undersaturation P/P^0. Figure 6 shows the isotherm for a slit of width $H^* = 20$. At low pressures, only one low density (vapour like) phase can be found in the pore. Upon increasing the pressure, the adsorption rises

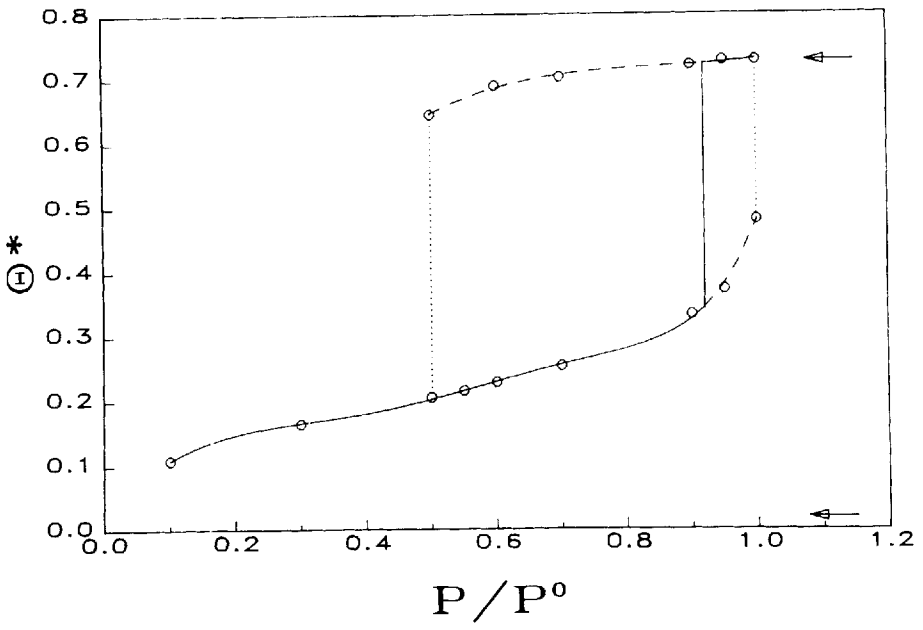

Figure 6 Adsorption isotherm Θ^* (P/P^0) at $T^* = 0.8$ in the slit of reduced width $H^* = 20$. The slit can be filled with a vapour-like (lower branch) or liquid-like (upper branch) phase. The solid lines pass through the *stable* phase at each pressure; the dashed lines through the metastable phases. The dotted lines show the beginning (at μ_{min}) and end (μ_{max}) of the metastable region. The arrows mark the coexisting vapour and liquid densities in the bulk fluid (at $P = P^0$). $\Theta^* \equiv \Theta\sigma_{ff}^3$ and $T^* \equiv k_B T/\varepsilon_{ff}$.

steadily until, at an undersaturation of around 0.45, a second, high density (liquid-like) phase appears. Both phases may be found for higher pressures until the vapour phase disappears at around P^0. Between these two points (corresponding to the limits μ_{min} and μ_{max} of the metastable region as described in §3) both phases are apparently stable in the pore. It has been argued elsewhere [18] that the vapour branch of the isotherm must terminate before P^0 if $T > T_W$; we note that our result is not inconsistent with this observation since, in the first place, the uncertainty in the equation of state (mentioned in §2.1, above) prevents our knowing P^0 to an accuracy of more than a few percent and, in addition, the vapour phase is only apparently stable at $P \simeq P^0$ for the duration of a few thousand steps of the simulation (see, e.g. figure 5).

Figure 7 shows the reduced grand potential per unit area Ω^*/A^* for the two phases in the metastable region. The error bars are estimated by calculating subaverages over 5000 steps. The statistics are poor, but it can be seen that the vapour phase is stable (i.e. has the lower Ω) at low pressures, while the liquid phase is stable at high pressures. The transition is at $P/P^0 = 0.92 \pm 0.05$. At this undersaturation the vapour-filled pore and the liquid-filled pore are in thermodynamic equilibrium. This is the point of capillary condensation.

In order to compare the phase behaviour in the pore with that in the bulk, the coexisting liquid and vapour densities [26] in the bulk phase (i.e. at P^0) at $T^* = 0.8$ have been marked on Figure 6. It can be seen that density of the liquid-filled pore is close to the density of the coexisting bulk liquid, while the pore vapour density is

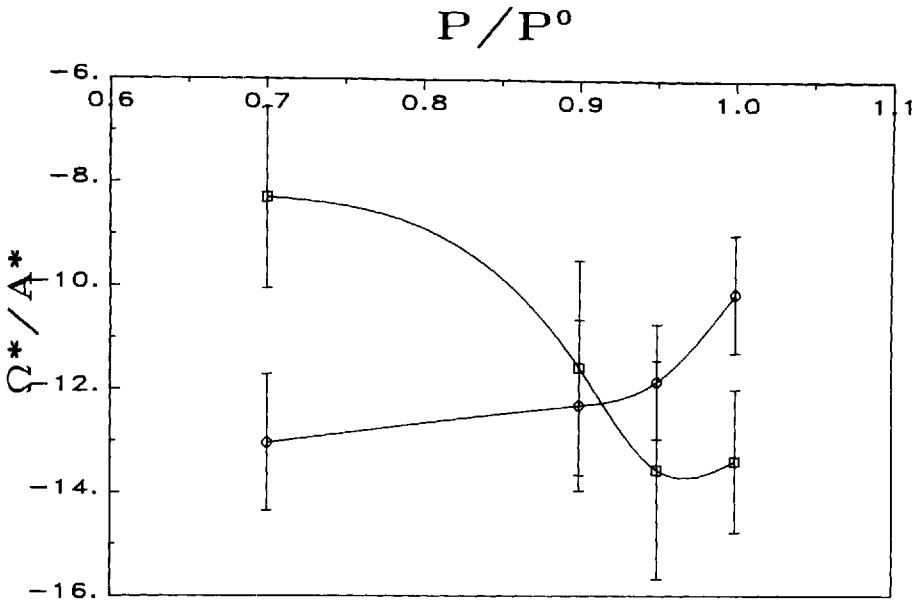

Figure 7 Reduced grand potential per unit area Ω^*/A^* as a function of fluid undersaturation in the $H^* = 20$ slit. Circles: vapour-like phase; squares: liquid-like phase. The error bars are estimated from subaverages over blocks of 5000 steps. $\Omega^*/A^* \equiv \Omega\sigma_{ff}^2/A\varepsilon_{ff}$.

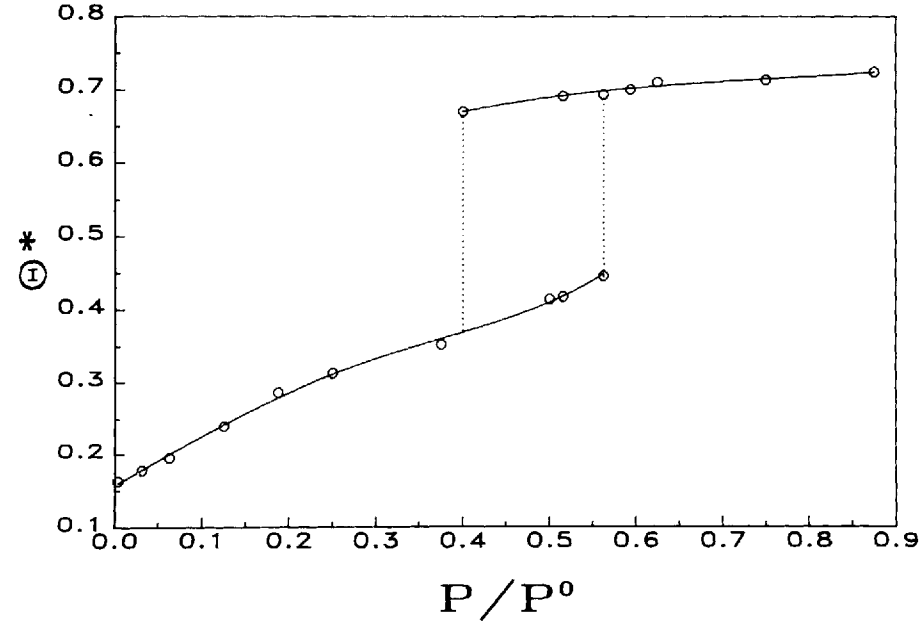

Figure 8 Adsorption isotherm at $T^* = 0.8$ in the $H^* = 10$ slit. The solid lines guide the eye through the simulated points; the dotted lines mark the limits of the metastable region.

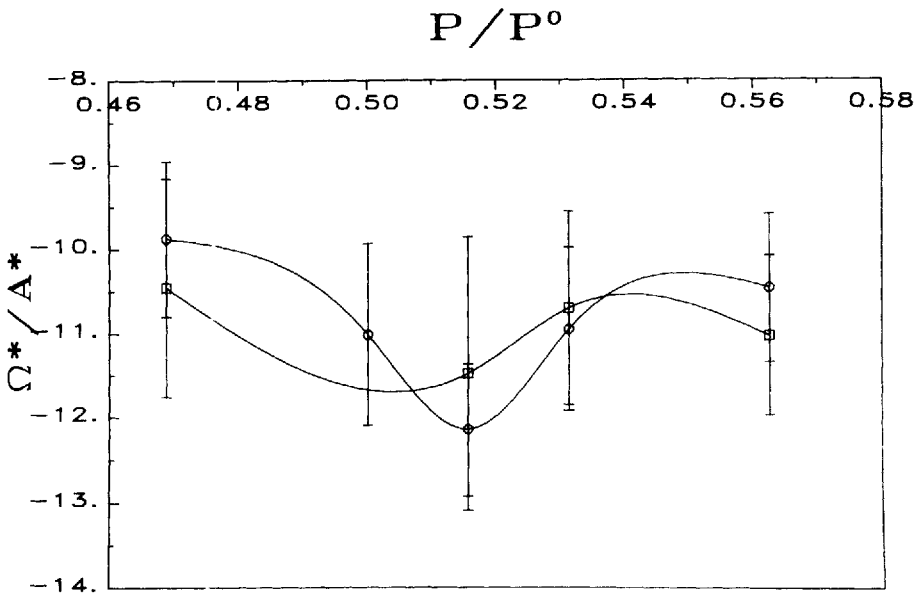

Figure 9 As Figure 7, but now for the slit with $H^* = 10$.

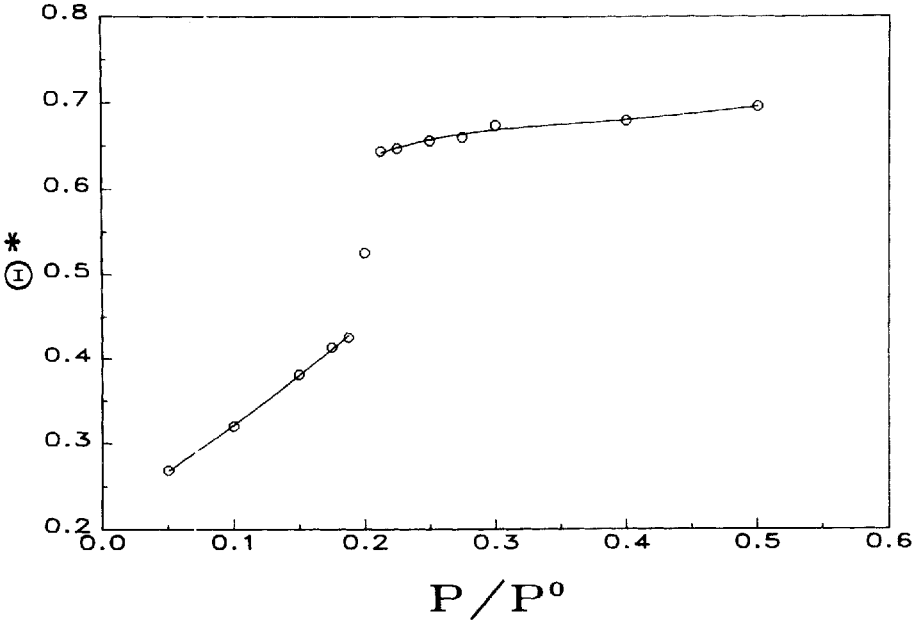

Figure 10 As Figure 8, but now for the slit with $H^* = 7$. The solid lines guide the eye through the vapour-like and the liquid-like branches of the isotherm. The steeply rising portion is centred on $P/P^0 \simeq 0.2$.

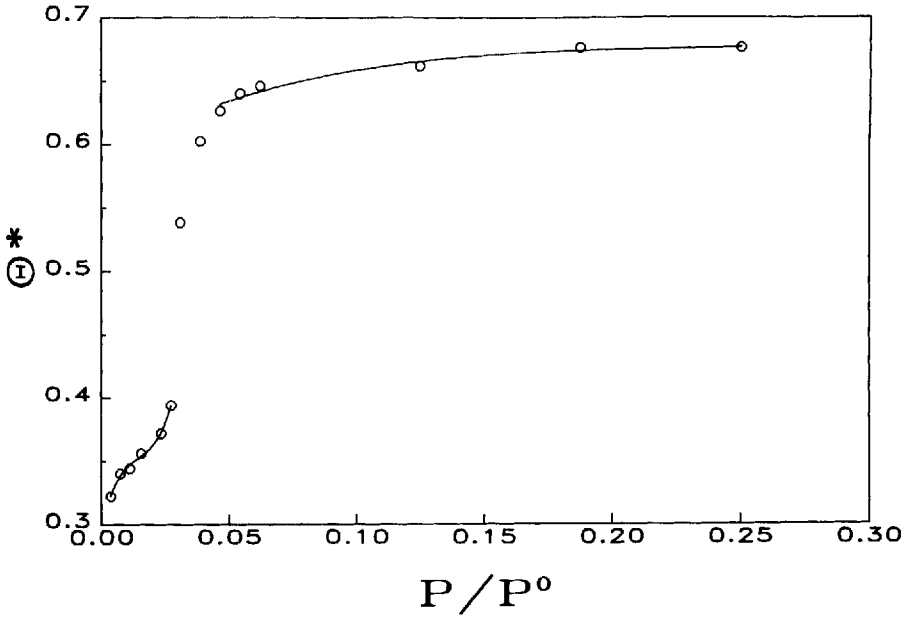

Figure 11 As Figure 10, but now for the $H^* = 5$ slit. The steep rise is centred on $P \simeq 0.03\ P^0$.

about two orders of magnitude greater than that of the coexisting bulk vapour, even at pressures as low as $0.1\ P^0$. The density enhancement due to the pore is clearly rather considerable. The steepness of the vapour branch of the isotherm (for this slit, and the smaller ones below) is suggestive of adsorption at a temperature in excess of T_w [18,19].

As the slit width is decreased ($H^* = 10$, Figure 8) the transition region moves to lower pressures. The vapour phase disappears at a lower pressure than in the larger slit, and so there is a range of pressures over which only the liquid phase is stable. The metastable region is now much smaller, and it is not possible to determine the point of capillary condensation because of the noise in the calculation of Ω (see Figure 9). The metastable region has disappeared altogether when the slit width is decreased still further to $H^* = 7$ (Figure 10) although the isotherm still exhibits a steep rise at around $0.21\ P^0$ which connects a low density and a high density part of the isotherm. The position of this rise shifts to even smaller pressures upon further reduction of the slit width ($H^* = 5$, Figure 11) – in this pore it occurs at $P/P^0 \simeq 0.03$.

The adsorption isotherm in a very narrow slit ($H^* = 3$) is shown in Figure 12. Upon decreasing the pressure to the extremely low value of $10^{-5}\ P^0$, the amount adsorbed drops sharply. We could find no evidence of a low density branch to the isotherm for this size of slit. Similar behaviour was observed at very low pressures in large pores. Thus, for example, the adsorption in the $H^* = 10$ slit remained constant (at the value shown as the intercept of the isotherm on the adsorption axis in Figure 8) down to extremely low pressures before dropping sharply at $P/P^0 = 6 \times 10^{-5}$. It thus seems as if there is some residual adsorption of the fluid in these larger pores which only disappears at very low pressures, and that, for very small pores, this

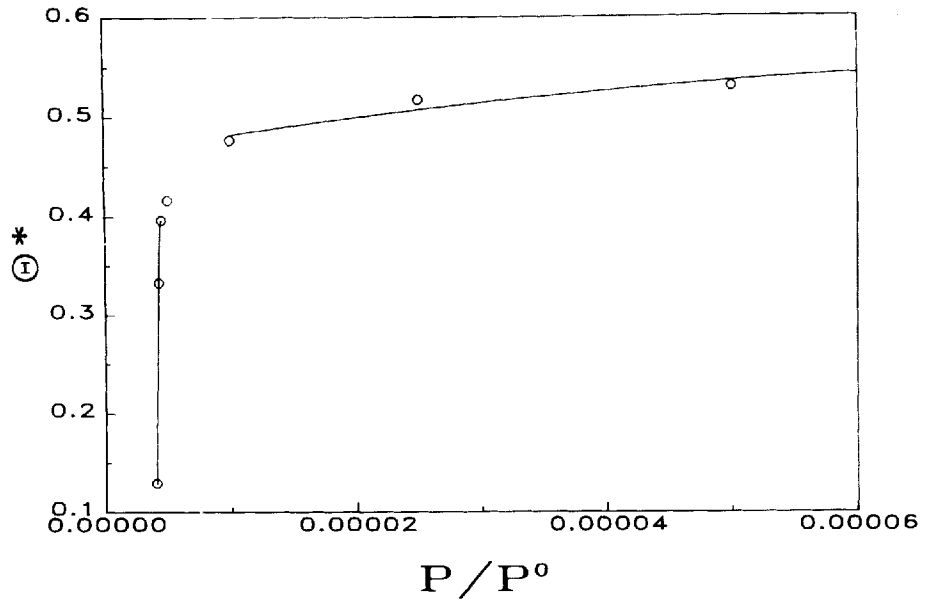

Figure 12 As Figure 1, but now for the slit with $H^* = 3$. The adsorption remains constant down to $P/P^0 = 10^{-5}$, where it drops sharply to (presumably) zero.

residual adsorption is all that can be observed. We return to this point in the following subsection, where we consider the structure of the fluid within the pore.

4.2 Structure of the Adsorbed Phase

Here, we discuss the simulation results for the reduced density profile $\rho^*(z^*)$ (defined in §3) and relate them to changes in the form of the adsorption isotherm (§4.1) as the slit width is altered.

Figure 13 shows a set of profiles in the slit with $H^* = 20$. These are at a series of pressures ranging from 0.1 to 0.9 P^0, or just below the point of capillary condensation in this slit (see Figure 6). All of the profiles plotted in this figure are from simulations corresponding to the vapour branch of the adsorption isotherm – i.e. the thermodynamically stable phase over this range of pressures. In Figure 13, we focus attention on the fluid in the neighbourhood of the walls of the slit (in this case, the left-hand wall at $z = 0$). There are strong oscillations in $\rho(z)$, due to the fluid packing in layers against the impenetrable wall. In particular, the first layer is very dense and strongly localised (note that way that ρ goes to zero on either side), which suggests that is is possibly *solid-like* in nature. (To determine whether or not the layer is indeed solid, the structure of the fluid in the plane of the walls would have to be studied in more detail [45].) The number of layers becomes larger as the pressure is increased, until at $P/P^0 = 0.9$, four (or – just possibly – five) layers have formed on each wall. We note that the $(i + 1)$th layer begins to form before the ith one is complete. This cooperative buildup of layers during adsorption has been previously observed by Snook and van Megen in their simulations of a LJ model of fluid ethylene in wide

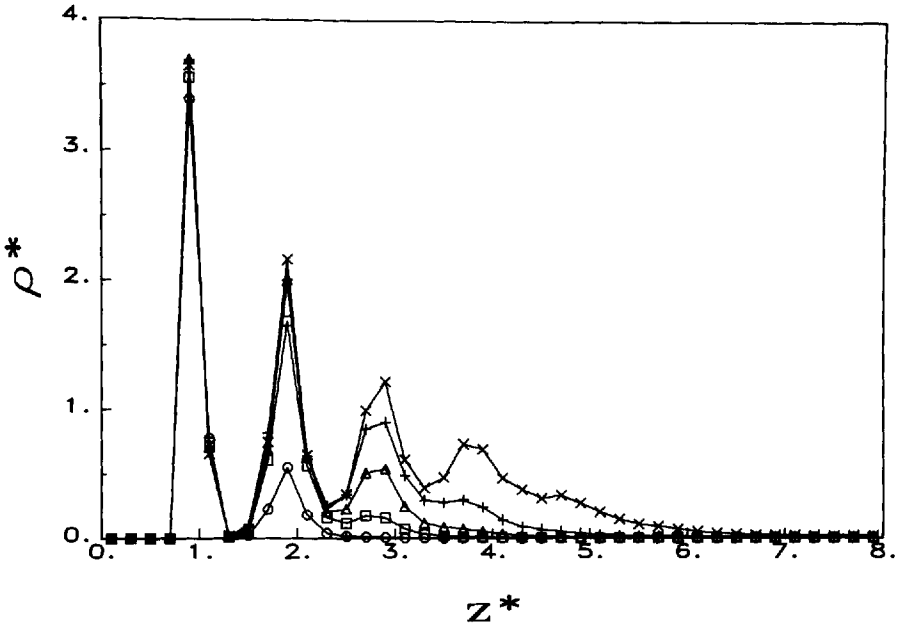

Figure 13 Reduced density profiles $\rho^*(z)$ at $T^* = 0.8$ in the $H^* = 20$ slit. $P/P^0 = 0.1$ (circles), 0.3 (squares), 0.5 (triangles), 0.7 (plusses) and 0.9 (crosses). At pressures which fall within the metastable region of the isotherm, the profile corresponding to the vapour phase is displayed. Only the parts of the profiles near the left-hand wall of the slit are shown $\rho^* \equiv \rho\sigma_{ff}^3$.

($H^* = 35$) graphite slits [46,47]. All of the profiles have a well-defined first peak, whose height is almost completely insensitive to presssure.

What happens to the structure of the fluid phase upon capillary condensation in this slit? The profiles of the vapour and liquid phases at pressures that are respectively just below and just above that of the transition are shown in Figure 14. It is immediately apparent that although the two phases are clearly of differing densities in the region around $z = H/2$ (in what may be termed a bulk-like region, far from the influence of the pore walls), the structure of the fluid close to the wall is the *same* for both phases. A similar result has been obtained (but not commented on) by van Megen and Snook [4]. It appears as though capillary condensation from vapour to liquid occurs, not in the space defined by the separation of the pore walls, but in the subregion between the inner edges of the adsorbed layers that form on the walls prior to condensation taking place.

Figure 15 shows the vapour density profiles near the left-hand wall of the slit with $H^* = 10$ for four pressures between $P/P^0 = 0.125$ and 0.156. The metastable region (which includes the point of capillary condensation, although it is not known which pressure this corresponds to) extends from 0.4 to 0.563 P^0 in this slit (see Figure 8). As in the larger slit (Figure 13) the oscillations in $\rho(z)$ form cooperatively (although now only three layers have appeared at the highest pressure) and the height of the first peak in $\rho(z)$ is independent of pressure. Figure 16 shows the vapour and liquid profiles at $P/P^0 = 0.516$, in the metastable region. Once again, it can be seen that the two phases differ only in their density in the bulk region near the centre of the pore; the

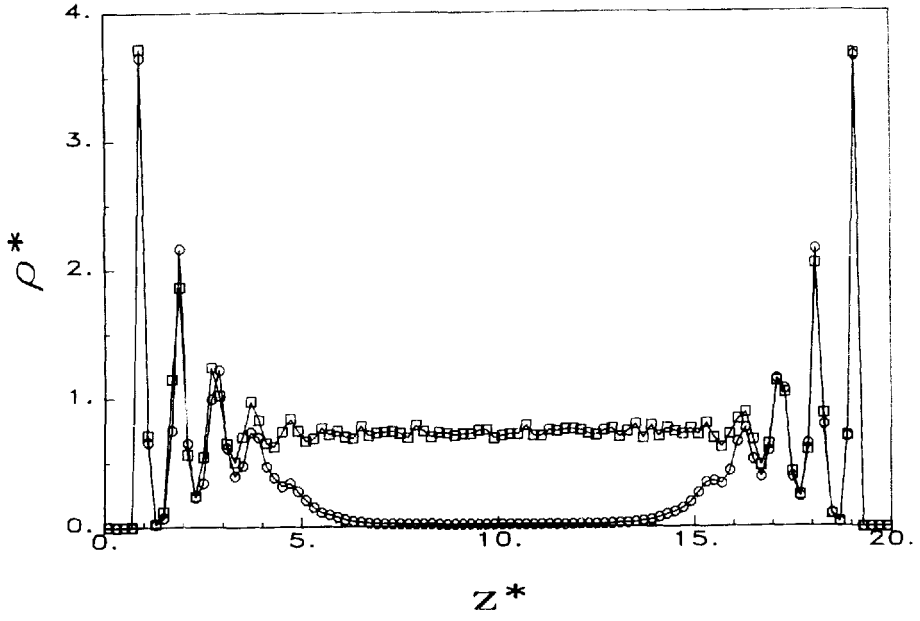

Figure 14 Reduced density profiles in the slit of Figure 13, but now for the whole slit with $P/P^0 = 0.9$ (circles) and 0.95 (squares). The point of transition between the stable vapour and liquid phases (i.e. capillary condensation) is at roughly $P/P^0 = 0.92$.

structure of the adsorbed layers near the walls does not depend on whether $\rho(H/2)$ has a vapour or liquid value.

Comparison of figures 14 and 16 shows that reducing H decreases the size of both the bulk region and the number of adsorbed layers that are insensitive to the phase there. Thus, in the larger slit ($H^* = 20$) the jump from vapour to liquid is associated with an increase in the fourth peak in $\rho(z)$ while for $H^* = 10$ this effect is seen in the third peak. It also appears from this comparison that the height of (for example) the first peak roughly doubles when the slit width is halved at fixed fluid undersaturation. We recall, however, that δ, the bin size for the calculation of $\rho(z)$, is proportional to H in our simulations (see §3, above) and so it is not possible to directly compare $\rho(z;H)$ for different values of H. The proper comparison is between the *integrals* of the profiles over the space occupied by each peak in the separate slits, which shows that the number of molecules in the first layer is rather insensitive to changes in H, while the number of molecules in the second, third etc. layers increase slightly as the slit is made smaller. This point is brought out rather more clearly when one considers Γ, the adsorption excess, as a function of H at fixed P/P^0 (see Table II). Γ may be thought of as being a measure of the thickness of the adsorbed layer on each wall (see the Table caption). In large slits, Γ is a constant, characteristic of an isolated solid-vapour surface at this pressure. As H is decreased, Γ rises monitonically, because of the enhancement of the attractive, long-ranged adsorption forces at the two walls of the slit. (We note in passing that, although it has not been seen here, it is possible to observe capillary condensation by fixing P/P^0 and varying H; this is the so-called "film

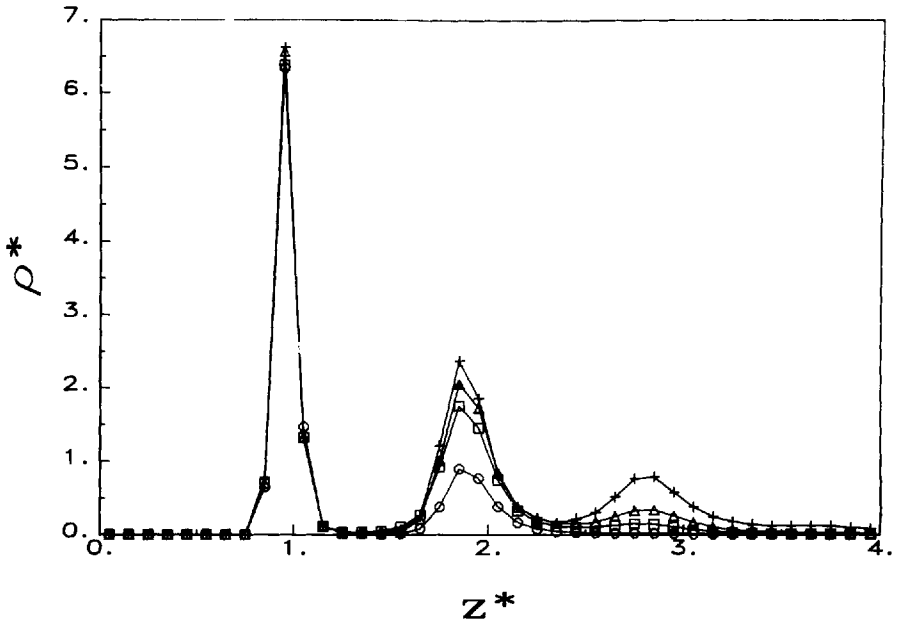

Figure 15 Reduced density profiles in the slit with $H^* = 10$. $P/P^0 = 0.125$ (circles), 0.250 (squares), 0.375 (triangles) and 0.516 (plusses). The profile at $P/P^0 = 0.516$ corresponds to the vapour-like phase in the pore. Only the parts of the profiles near the left hand-wall of the slit are shown.

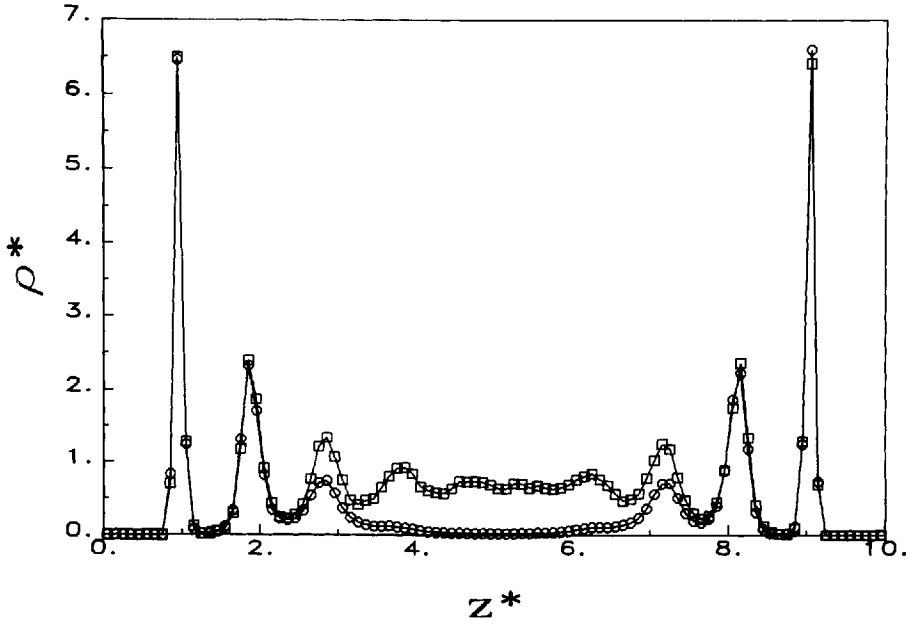

Figure 16 Reduced density profiles corresponding to the vapour-like (circles) and liquid-like (squares) phases in the $H^* = 10$ slit at $P/P^0 = 0.516$.

Table II Adsorption excess at $P/P^0 = 0.5$.

H^*	Γ^*
7	2.40 (2)
10	2.02 (7)
20	1.98 (7)
40	1.91 (5)
60	1.96 (5)

Reduced adsorption excess $\Gamma^* = \Gamma\sigma_{ff}^2$ (see §3) in pores of various reduced widths H^* at $T^* = 0.8$ and $P/P^0 = 0.5$. The figures in brackets are the estimated uncertainty in the last decimal place. Assuming that the film of adsorbed phase at the wall is of uniform density ρ_l^* (the reduced bulk liquid phase density at bulk coexistence), Γ^* may be converted to an equivalent reduced film thickness by dividing by $\rho_l^* = 0.72$ [26].

snapping" transition which was found by Lane and Spurling [3]. In this work, we have chosen to do it the other way round, since this corresponds more closely to a real adsorption experiment.)

As H is reduced, the bulk region eventually disappears as the layered structures on each wall coalesce. Profiles in the slit with $H^* = 7$ are displayed in Figure 17. At most six (three on each wall) layers can fit into the pore. Some degree of cooperative formation is still apparently present in the layers that are close to the wall. We can now see that the steep rise in Θ displayed in Figure 9 is due to a rapid increase in the height of the third peak in $\rho(z)$. Once again, the structure of the (four) remaining adsorbed layers close to the wall is insensitive to pressure, both before and after this change. That is, the space in which the density increase in this pore is occurring is still only the subregion between these adsorbed layers, as opoposed to the space between

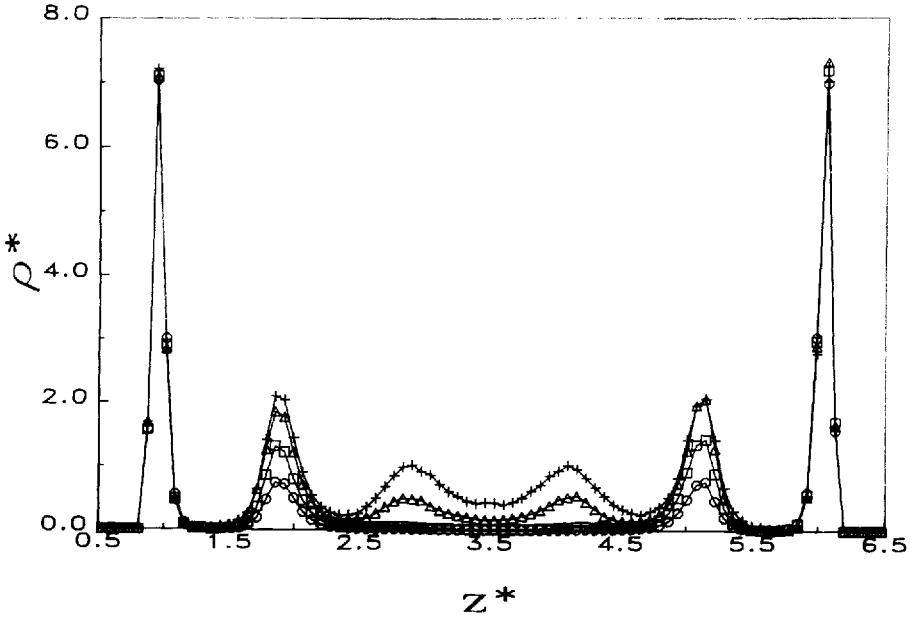

Figure 17 Reduced density profiles in the slit with $H^* = 7$. $P/P^0 = 0.10$ (circles), 0.15 (squares), 0.20 (triangles) and 0.25 (plusses). A steep rise in the adsorption isotherm occurs at $P/P^0 \simeq 0.2$.

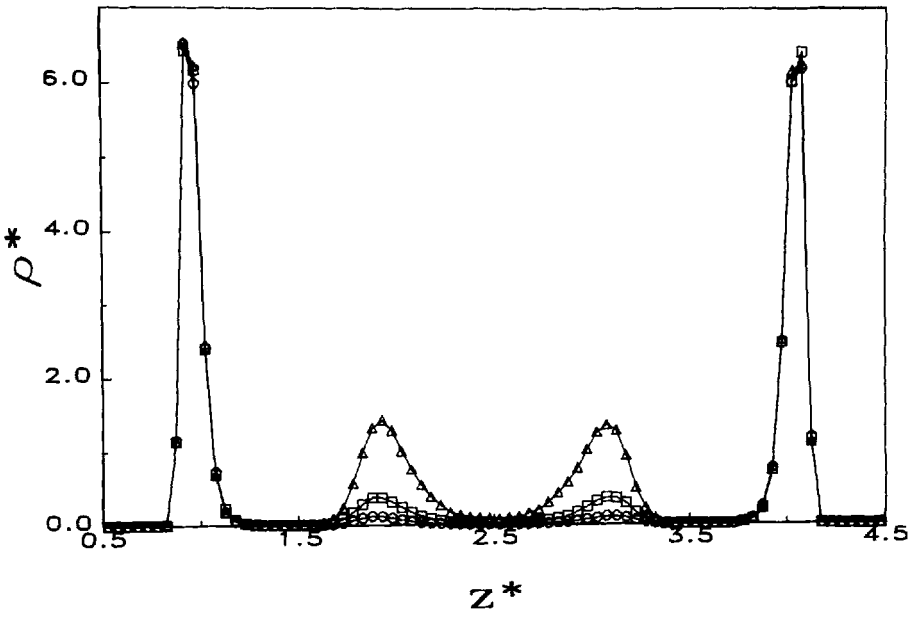

Figure 18 Reduced density profiles in the $H^* = 5$ slit. $P/P^0 = 0.0156$ (circles), 0.0273 (squares) and 0.0313 (triangles). A steep rise in the isotherm occurs at $P/P^0 = \simeq 0.03$.

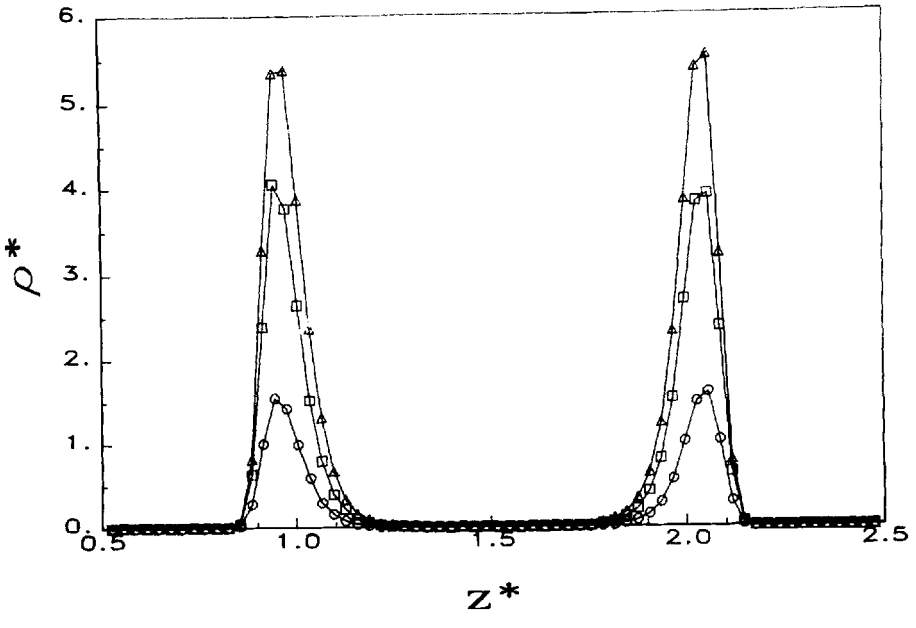

Figure 19 Reduced density profiles in the slit with $H^* = 3$. $P/P^0 = 4 \times 10^{-6}$ (circles), 4.25×10^{-6}, (squares) and 10^{-5} (triangles).

the pore walls. This trend continues upon going to smaller pores. Four layers are present when $H^* = 5$ (Figure 18) and the increase in the adsorption isotherm now corresponds to a change in the height of the second peak, while the size of the peaks in $\rho(z)$ closest to the wall is independent of pressure.

Finally, a pore may be so small ($H^* = 3$) that only two layers can fit into the space between the walls. These are present at – essentially – all pressures, since it is only going to extreme low pressures that any reduction in their density can be observed. The reduction in peak height (shown in Figure 19) then takes place (at $P/P^0 \simeq 10^{-5}$) over a very narrow range of pressure and is responsible for the sudden drop in the adsorption isotherm for this slit (Figure 12). This first layer of adsorbed molecules at the pore wall are responsible for the residual adsorption in larger slits that has been previously mentioned (§4.1). It appears as if, for this system, the walls of all pores (large and small) are coated with a layer of adsorbate at all but the very smallest of pressures. The solid-like nature of the well-defined layers at the wall may be examined in a little more detail in this extreme case where only two of them are present; we find that their two-dimensional density is typically 65% of the density of the close-packed 2D solid.

The ideas developed in this subsection concerning the structure of the fluid within the pore may be reinforced by looking at "snapshot" pictures [48,49] of configurations from (say) the runs at $H^* = 20$,10 and 7 (figures 20–22). We show both liquid-like and vapour-like configurations from each of these simulations. The snapshots clearly reveal the well-defined layering at the wall, the insensitivity of this structure to the density in the centre of the pore, and the way in which the layers on the walls merge as the pore is made smaller.

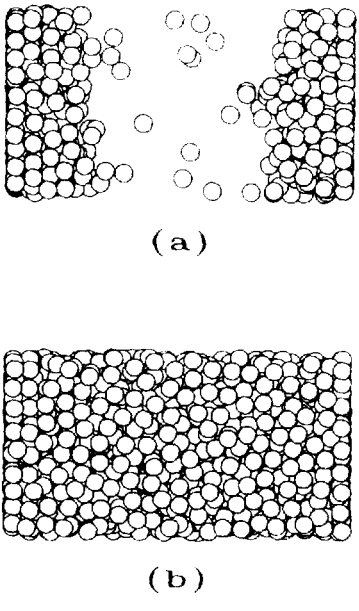

Figure 20 Snapshot images [48,49] of configurations from the simulations in the $H^* = 20$ slit at $P/P^0 =$ (a) 0.90 and (b) 0.95. (See colour plate VII.)

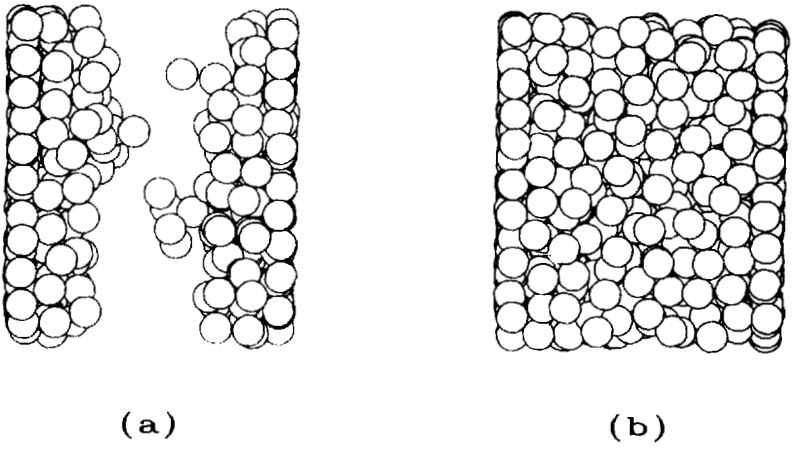

Figure 21 As figure 20, but now for the $H^* = 10$ slit. (a) is the vapour-like phase, (b) the liquid-like phase at $P/P^0 = 0.516$. (See colour plate VIII.)

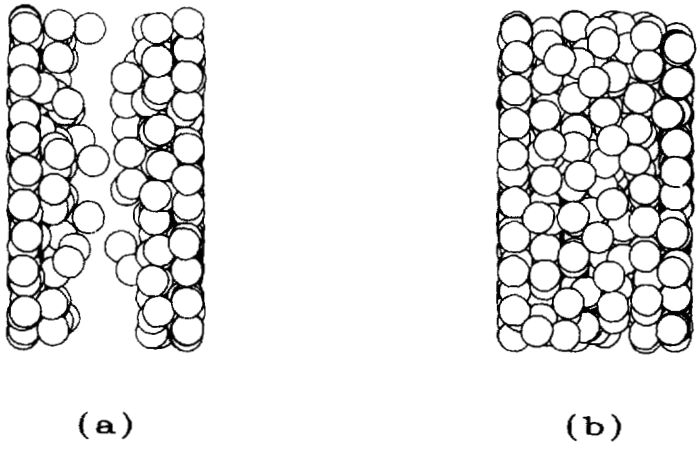

Figure 22 As figure 20, but now for the slit with $H^* = 7$. $P/P^0 =$ (a) 0.1875 and (b) 0.2125. (See colour plate IX.)

5. DISCUSSION

5.1 Summary of Results

The simulation results that have been presented in this paper provide a rather direct picture of the mechanisms involved in capillary condensation in our model system. Here, we summarise this picture, before concentrating on the significance of the metastable states in large pores (§5.2) and the range of applicability of the thermodynamic equations for the capillary coexistence curve (§5.3). In discussing our results, it will be convenient to distinguish between *three* ranges of pore size, which will be defined below in terms of H^*. Our division is unrelated to the traditional micro/meso/macro division of §1 (above) which is made in terms of absolute pore

sizes; furthermore we would expect the absolute positions of the boundaries between our ranges to be sensitive to the details of the fluid-fluid and solid-fluid potentials employed in the simulations (see §6, below). *Large pores* have widths of the order of ten molecular diameters or more. A fluid molecule inside a large pore will find itself either within one of the layers formed by the packing of the fluid against the pore wall, or in a bulk region, further away from the walls. As the pressure is raised, the layers grow cooperatively, which is made manifest as a *steady* increase in the amount of fluid adsorbed. The density of the bulk region can be either low (in which case the pore can be described as being filled with vapour) or high (when the pore is filled with liquid). The liquid branch of the isotherm is flatter than the vapour branch, because of the liquid's lower compressibility and the effect of layer growth on the vapour branch. Liquid-filled large pores begin to appear at pressures greater than $\sim 0.5\ P^0$, while vapour-filled pores can exist at pressures greater than this value. Thus, there is a metastable region surrounding the point of capillary condensation, which is the transition between the stable phases, and which can be seen as a sudden jump in the amount of adsorbed fluid. The structure of the adsorbed layers at the wall do not change at condensation, but the transition takes place in the space between the inner adsorbed layers (as opposed to the space between the pore walls). Decreasing the pore-size shifts the point of capillary condensation to lower pressures and decreases the size of the metastable region.

As the pore becomes smaller, we enter the realm of *medium* pore sizes ($3 \lesssim H^* \lesssim 10$). Now the bulk region in the centre of the pore has vanished and all the structure of the confined fluid is dominated by the layering effects induced by the walls. The layers closest to the wall still fill in a cooperative manner with increasing pressure, which again shows up as a steady rise in the adsorption isotherm. The low density branch of the isotherm is shorter and steeper than the vapour branch in large-pore isotherms. No metastable states are to be found in medium pores; instead, the isotherm is reversible with a very steep portion which connects the low and high density branches. In the system studied here, the rapid increase in the isotherm (at $\lesssim 0.5\ P^0$) is due to a change in the density of the inner layers; the structure of the layers closer to the walls is the same on both branches of the isotherm.

Small pores have sizes of the order of three molecular diameters or less. Their adsorption characteristics are dominated by the properties of the strongly-localised, high density (possibly solid-like) layer of fluid molecules on each wall. These layers appear at extremely low pressures and, thereafter, are almost completely insensitive to changes in pressure. Since the pore is full at (practically) all pressures, the isotherm is flat, with no jumps, risers or any other features.

5.2 *Metastable States*

The chief difference between the isotherms for large and medium pores in this study is that the former exhibit a vertical jump between well-defined vapour and liquid branches with an attendant metastable region, while the latter do not. Before discussing the significance of the presence of metastable states in large pores, it is worthwhile to interpose some comments on their status. It is well-known that the finite nature of the (a) length of the run and (b) simulation cell can result in the appearance of metastabilities in the neighbourhood of a first-order phase transition. With regard to (a), we recall that in this work, th size of the metastable region has been determined by tracking down the limits in μ ($\mu_{\min}$ and $\mu_{\max}$, see §3 and Figure 5, above) for which,

over the lifetime of the run, it is possible to observe crossings from the metastable state to the stable one. It is thus plausible that the apparant metastable region would become smaller (i.e. μ_{min} would increase and/or μ_{max} would decrease) if the simulations were run for longer. Whether or not the metastable region would, in the limit of an infinitely long run, disappear altogether is not known.

Although we have not looked in detail at the way in which the metastable region changes with the size (i.e. cross-sectional area, A) of the cell, we have, as noted in §3 above, made a limited study of the dependence of Θ and Ω upon A. Those runs were performed at $P/P^0 = 0/516$ and $H^* = 10$, which gives both liquid and vapour states, at $A^* = 100$, although it cannot be determined which is more stable. This remains the case upon increasing A^* to 200 or decreasing it to 75, but at $A^* = 50$, the liquid state is more stable than the vapour, while for $A^* = 25$, only the liquid state was found. It therefore seems as if the details of the phase equilibria (and hence, the metastabilities) are sensitive to system size for areas that are somewhat smaller than the one which we have chosen to use in this work, but that there is apparantly little qualitative change upon going to larger A.

The disappearance of the adsorption jump and the metastable states as H is reduced suggests that the capillary coexistence curve terminates at a capillary critical point, (H_C, P_C) [8–16, 18–20,23]. From the results presented here (and bearing in mind the remarks above concerning the status of our observations of metastabilities) we estimate a *lower bound* on H_C^* in our system to be about 7 at this temperature, while the corresponding estimate for the minimum value of P_C^* is roughly $0.25\,P^{0}{}^*$. For $H < H_C$ (or $P < P_C$), capillary condensation does not occur; instead, the isotherm is reversible with a rapid rise in density which takes place over a rather small range of pressures. It might be thought that the appearance of the metastable states (i.e. subcriticality) in the isotherm and the presence of the bulk region in the centre of the pore were somehow linked together, since both are present for $H^* = 10$ and 20, but not for $H^* = 7$ and 5. However, it is not clear whether this is true in general – i.e. at other temperatures. Density functional calculations of the capillary phase diagram [16,18] show $P_C(T)/P^0 \to 1$ and $H_C(T) \to \infty$ as $T \to T_C^{(3)}$ – at least for $T/T_C^{(3)} \sim 1$. Thus, increasing T in our system would, according to this picture, increase H_C and it is possible that this could move into the regime where pores exhibit a bulk-like region at their centres. Indeed, Peterson and Gubbins [8] have shown a supercritical density profile (albeit for Ar in a cyinder of solid CO_2) that displays a bulk-like region, which tends to confirm our suspicion that there is in fact no connection between the bulk region and the position of the critical point.

The appearance of metastable states is of interest because of their possible connection with hysteresis effects in the sorption isotherm [18,19,21,50]. Thus, looking at Figure 6, for example, it is possible to imagine an adsorption (increasing P) experiment following the vapour branch, past the point of capillary condensation at $P/P^0 \simeq 0.92$, up to where the metastable portion of the branch ends at $P \simeq P^0$. A desorption (decreasing P) experiment would then follow the liquid branch, down past the capillary condensation pressure until the metastable part ends at $P/P^0 \simeq 0.5$, when it would switch to the vapour branch, which it would follow down to zero pressure. Neither on the adsorption branch nor on the desorption branch would the jump between vapour and liquid occur at the point of thermodynamic equilibrium between the two phases. Such a sorption isotherm would thus exhibit hysteresis – indeed, it would be qualitatively identical with the isotherm for a predominantly mesoporous adsorbent which we have sketched in Figure 1. By contrast, a continuous,

supercritical isotherm (Figure 11, for example) is very similar in form to the schematic microporous isotherm of Figure 2, bearing in mind that the gas branch for small pores can be very short (and, in the case of our system, will vanish altogether for $H^* = 3$). Thus, it is plausible to suggest [52,18,19] the existence of a link between the critical capillary size H_C and the boundary between mesopores and micropores, since the former exhibit hysteresis while the latter do not. It should be noted that, according to this picture, the position of the meso/micropore boundary is a function of T and so it should in principle be possible to induce changes in the hysteretic behaviour of a (suitably chosen) adsorbent by measuring several sorption isotherms at a variety of temperatures.

We emphasise that this mechanism for hysteresis, which links it to whether H is above or below H_C is based on the *single, isolated, well-defined* pore model which we have used. Pore connectivity and polydispersity in pore sizes have conventionally been invoked [1] to explain hysteresis in sorption experiments on porous solids. Whilst there can be no doubt that these properties will induce hysteresis [1,21,51] the point of view described here and elsewhere [18–20, 8–11] asserts that such effects are *additional* to the hysteresis exhibited by individual pores. In addition, the pore geometry is often thought to be an important factor in the appearance of hysteresis. Thus, "ink-bottle" and conical capillaries are sometimes thought to exhibit hysteresis, while other geometries do not [1]. Although the shape of the capillary will doubtless influence the quantitative details of capillary condensation, our results show that it is *not necessary* to resort to exotic pore shapes to explain hysteresis in adsorption isotherms.

5.3 *The Kelvin and Laplace equations*

Evans and Marini Bettolo Marconi [17] have shown how consideration of the grand potential of vapour and liquid configurations in the pore leads to the *Laplace equation* for P, the pressure at which capillary condensation of vapour to liquid occurs:

$$P - P_l^+ = 2\gamma_{lv}\cos\theta/H \tag{12}$$

Here, P_l^+ is the pressure of the metastable bulk liquid phase which is at the same T and μ as the vapour, while γ_{lv} is the surface tension of the liquid-vapour interface. θ is the angle of contact between the liquid phase and the solid wall of the pore; recall that it is zero for $T \geqslant T_W$ and positive for $T < T_W$. For $P \sim P^0$ and, assuming the vapour to be close to ideal, (12) reduces to

$$k_B T \ln(P^0/P) = 2\gamma_{lv}\cos\theta/H(\rho_l - \rho_v) \tag{13}$$

the more familiar *Kelvin equation*, where ρ_l and ρ_v are the densities of the bulk liquid and vapour phases at coexistence (i.e., at P^0). As noted in §1, this equation may be used to predict the capillary coexistence curve (i.e. P as a function of H) from a knowledge of the contact angle and the liquid-vapour interfacial properties and it has therefore received a good deal of attention, some of which concerns its range of validity [1,8,9,11,16,18,19]. The Laplace equation may also be used to predict the coexistence curve, provided (as is the case here) an equation of state which links P and P_l^+ is available.

Figure 23 displays the simulation results for the capillary condensation pressure as a function of pore size for the large pores, together with the pressures at which the rapid increase in density occurs in the medium pores. (For $H^* = 10$, we have

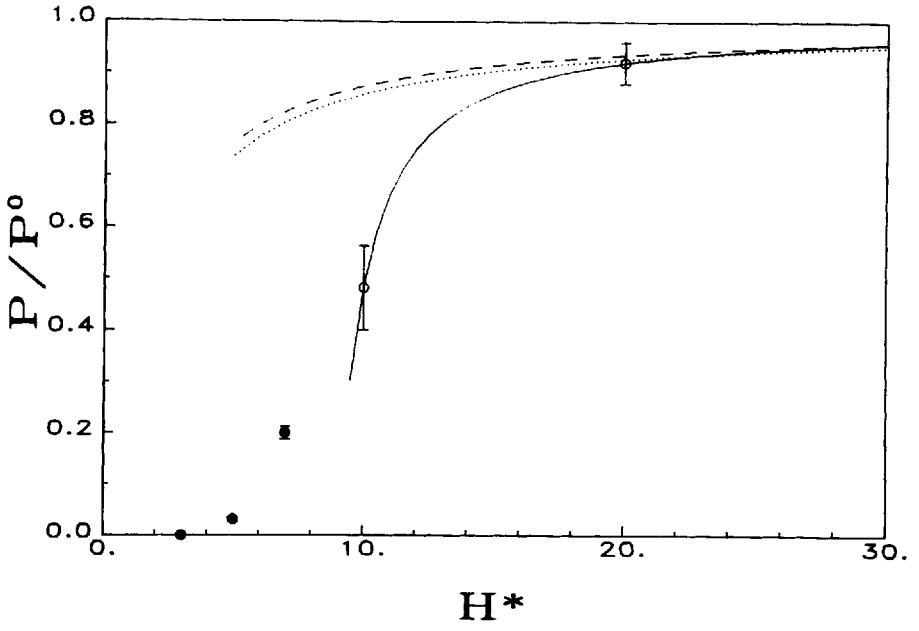

Figure 23 Capillary phase diagram at $T^* = 0.8$. The open circles (with error bars) give the pressures at which (for fixed H^*) capillary condensation takes place in the larger pores – i.e. $H^* > H_C^*$, where (H_C^*, P_C^*) is the location of the capillaary critical point. The filled circles indicate the positions of the steep rise in the isotherms for $H^* < H_C^*$, $P^* < P_C^*$. The dotted curve is the prediction of the Laplace equation (14), while the dashed curve is the prediction of the Kelvin equation (15). The full curve is the empirical fit of (16) with a = 0.941 and b = 8.71, through the two points at $H^* = 10$ and 20.

arbitrarily put P/P^0 equal to the midpoint of the pressure range of the metastable region). Also shown in the prediction of (12) and (13):

$$P/P^0 = (P_l^{+}{}^* + 2\gamma^*{}_{lv}/H^*)/P^{0*} \tag{14}$$

$$P/P^0 = \exp[-2\gamma^*{}_{lv}/T^*(\rho_l^* - \rho_v^*)H^*] \tag{15}$$

($P^* \equiv P\sigma_{ff}^3/\varepsilon_{ff}$, the reduced pressure) where we have set $\cos\theta = 1$ and used the following parameter values [26,53]

$$\rho_l^* = 0.72,\ \rho_v^* = 0.02,\ \gamma_{lv}^* = 0.38$$

Here, the value for γ_{lv}^* ($\equiv \gamma_{lv}\sigma_{ff}^2/\varepsilon_{ff}$) has been estimated by subtracting the (substantial) potential truncation correction from the full LJ result [53]. Figure 23 shows that, over this range of P/P^0, the Kelvin prediction is typically only $\sim 1\%$ larger than the Laplace result. Both the Kelvin and Laplace predictions are in very good agreement with the simulation result at the larger H^*, but not at the lower; we find that the thermodynamic equations overestimate P/P^0 for smaller slits, in accordance with previous results obtained via density functional theory [16,18,19] and simulation [8–11] for $T > T_W$. The other curve in Figure 23 is a Kelvin-type expression

$$P/P^0 = \exp[-a/(H^* - b)] \tag{16}$$

which has been fitted to the two simulated points. If (16) is used to interpolate between

the two points, it appears that (14) or (15) begins to break down at $H^* \sim 16$. At $H^* = 10$, the thermodynamic equations predict a pressure that is roughly 80% too high and, bearing in mind the approximate location of the capillary critical point (see §5.2, above) and the shape of (16), we may estimate their maximum deviation to be (very approximately) 100% of the true transition pressure.

In the above treatment, we have allowed for the fact that $T > T_W$ by putting $\theta = 0$. The effect of the appearance of the wetting films (which decrease the effective slit width at condensation – see, e.g. figure 14) has not been explicitly included, however. For large pores, thick films and $P/P^0 \sim 1$, Evans and Marini Bettolo Marconi have argued that for fluid-wall potentials – such as the one used here – which decay as $-z^{-3}$, H should be replaced by $H - 3t_0$, where t_0 is the equilibrium film thickness at condensation [17]. Modifing the slit width in this way has little effect on the predictions of (14) or (15), since both curves are rather flat for $H^* \gtrsim 10$. Thus, if we take $t_0^* = 4$ for the $H^* = 20$ slit (Figure 14), the Laplace and Kelvin predictions for P/P^0 are reduced to 0.909 and 0.845, which are both slightly less than the simulated result, although still within its estimated error. The other slit ($H^* = 10$) is beyond the range of applicability of the modified Kelvin and Laplace Equations.

Using the density functional theory, Evans *et al* report the breakdown of (12) and (13) at $H^* \gtrsim 100$ [18] for complete wetting conditions. They note that the predictions are improved somewhat on going to the modifications of [17], but give the impression that, for $T > T_W$, the Kelvin and Laplace equations perform poorly, in general. Similar conclusions have been reached for cylindrical pores [11,19,20]. A direct comparison between density functional theory and simulation is precluded by differences in their bulk phase properties [22,8,11] and, in the absence of data for other pore sizes, it is difficult to say whether or not the agreement between the thermodynamic predictions and our simulation result at $H^* = 20$ is merely specious. However, Evans *et al* [18] note that, on going to a more attractive wall potential, the range of applicability of (12) is increased. Thus, the fact that the transition at $H^* = 20$ occurs rather close to P^0 (presumably as a result of our comparatively deep pore-fluid potential – see §2.1) may account for the agreement between the Laplace and Kelvin equations and our simulation.

6. CONCLUSIONS

In this paper we have presented details of an extensive molecular simulation study of the phase behaviour of a simple fluid confined to a slit-like pore formed from two parallel adsorbing walls. The temperature of our study is believed to be above both $T_C^{(2)}$ (so that 2D liquid-vapour coexistence is not observed as $H \to 0$) and T_W (so that thick wetting layers develop on the wall as $P \to P^0$). Our attention has been focussed on the way in which the (capillary) condensation of the bulk vapour to a adsorbed liquid-like phase is affected by the size of the pore. Large pores exhibit metastable liquid and vapour states and the point at which the two states are in thermodynamic equilibrium is identified by calculation of the system grand potential. The point of capillary condensation shifts to lower pressures as the pore is made smaller and disappears at a critical point (H_C, P_C), although pores which are smaller than the critical size continue to exhibit steeply rising portions. The differences between subcritical and supercritical isotherms are similar to those which exist in experimental isotherms for mesoporous and microporous adsorbents.

For the system studied in this paper, we estimate $H_C^* \gtrsim 7$ and $P_C/P^0 \gtrsim 0.25$. We also find that the density jump which occurs at condensation is localised to a bulk-like region in the centre of the pore and that the nature of the adsorbed layers at the pore walls is independent of whether the pore is filled with vapour or liquid. A purely thermodynamic description of the phase equilibria within the pore (such as the Laplace or Kelvin equation for the pressure at which capillary condensation occurs) breaks down (as it must on quite general grounds) as the pore is made smaller; here, we estimate that it is in poor agreement with our simulated results for $H^* \lesssim 16$, or well within the mesopore regime.

Finally in this paper, we comment on the generality of the picture of capillary condensation which has emerged from this and other studies. Using a density functional theory, we have made some investigations of the sensitivity of the results to changes in the fluid-fluid and solid-fluid potential parameters [54]. Preliminary results from that work indicate that the qualitative features of our results are not sensitive to the details of the model potential, but that the absolute values of (for example) the pore size at the critical point or at the boundary between the different ranges of H which we identified at §5.1 can depend quite strongly on the potential parameters which have been chosen for the model.

Acknowledgements

We thank W. van Megen, D. Nicholson and R. Evans for useful discussions and the British Petroleum Company PLC for permission to publish this work.

References

[1] S.J. Gregg and K.S.W. Sing, *Adsorption, Surface Area and Porosity* 2nd, edn., Academic Press, New York, (1982).
[2] N. Quirke, "Molecular simulation: progress and prospects", *Fluid Phase Equil.* **29**, 283 (1986).
[3] J.E. Lane and T.H. Spurling, "Monte Carlo simulation of the effects of adsorption on interparticle forces", *Aust. J. Chem.*, **33**, 231 (1980).
[4] W. van Megen and I.K. Snook, "Physical adsorption of gases at high pressure III. Adsorption in slit-like pores", *Mol. Phys.*, **54**, 741 (1985).
[5] D.W. Hawley, J.M.D. MacElroy, J.-C. Hajduk and X.B. Reed, "Monte Carlo simulation of two interacting liquid/vapour interfaces", *Chem. Phys. Lett.*, **117**, 154 (1985).
[6] B.K. Peterson, J.P.R.B. Walton and K.E. Gubbins, "Microscopic studies of fluids in pores: computer simulation and mean-field theory", *Int. J. Thermophys.*, **6**, 585 (1985).
[7] B.K. Peterson, J.P.R.B. Walton and K.E. Gubbins, "Fluid behaviour in narrow pores", in *Fundamentals of Adsorption*, ed. A.I. Liapis, Engineering Foundation, New York, 1987, p463.
[8] B.K. Peterson and K.E. Gubbins, "Phase transitions in a cylindrical pore. Grand canonical Monte Carlo, mean field theory and the Kelvin equation", *Mol. Phys.*, **62**, 215 (1987).
[9] G.S. Heffelfinger, F. van Swol and K.E. Gubbins, "Liquid-vapour coexistence in a cylindrical pore", *Mol. Phys.*, **61**, 1381, (1987).
[10] A.Z. Panagiotopoulos, "Adsorption and capillary condensation of fluids in cylindrical pores by Monte Carlo simulation in the Gibbs ensemble", *Mol. Phys.*, **62**, 701 (1987).
[11] B.K. Peterson, K.E. Gubbins, G.S. Heffelfinger, U. Marini Bettolo Marconi and F. van Swol, "Lennard-Jones fluids in cylindrical pores: Nonlocal theory and computer simulation", *J. Chem. Phys.*, **88**, 6487 (1988).
[12] D. Nicholson, "Molecular theory of adsorption in pore spaces. Part 1. – Isotherms for simple lattice models", *J. Chem. Soc. Faraday Trans. I*, **71**, 238 (1975).
[13] D. Nicholson, "Molecular theory of adsorption in pore spaces. Part 2. – Thermodynamic and molecular lattice model descriptions of capillary condensation", *J. Chem. Soc. Faraday Trans. I*, **72**, 29 (1976).

[14] M.E. Fisher and H. Nakanishi, "Scaling theory for the criticality of fluids between plates", *J. Chem. Phys.*, **75**, 5857, (1981).
[15] H. Nakanishi and M.E. Fisher, "Critical points shifts in films", *J. Chem. Phys.*, **78**, 3279 (1983).
[16] R. Evans and P. Tarazona, "Theory of condensation in narrow capillaries", *Phys. Rev. Lett.*, **52**, 557 (1984).
[17] R. Evans and U. Marini Bettolo Marconi, "The role of wetting films in capillary condensation and rise: Influence of long-range forces", *Chem. Phys. Lett.*, **114**, 415 (1985).
[18] R. Evans, U. Marini Bettolo Marconi, and P. Tarazona, "Fluids in narrow pores: Adsorption, capillary condensation and critical points", *J. Chem. Phys.*, **84**, 2376 (1986).
[19] R. Evans, U. Marini Bettolo Marconi, and P. Tarazona, "Capillary condensation and adsorption in cylindrical and slit-like pores", *J. Chem. Soc. Faraday Trans. II*, **82**, 1763 (1986).
[20] B.K. Peterson, J.P.R.B. Walton and K.E. Gubbins, "Fluid behavior in narrow pores", *J. Chem. Soc. Faraday Trans. II*, **82**, 1789.
[21] P.C. Ball and R. Evans, "On the mechanism for hysteresis of gas adsorption on mesoporous substrates", *Europhys. Lett.*, **4**, 715 (1987).
[22] J.P.R.B. Walton and N. Quirke, "Modelling the phase behaviour of a fluid within a pore", *Chem. Phys. Lett.*, **129**, 382 (1986).
[23] P. Tarazona, U. Marini Bettolo Marconi and R. Evans, "Phase equilibria of fluid interfaces and confined fluids. Nonlocal versus local density functionals", *Mol. Phys.*, **60**, 573 (1987).
[24] D.E. Sullivan and M.M. Telo da Gama, in *Fluid Interfacial Phenomena*, ed. C.A. Croxton, Wiley, New York, 1985, p45.
[25] P. Tarazona, "Free energy density functional for hard spheres", *Phys. Rev. A*, **31**, 2672 (1985).
[26] J.J. Nicolas, K.E. Gubbins, W.B. Street and D.J. Tildesley, "Equation of state for the Lennard-Jones fluid", *Mol. Phys.*, **37**, 1429 (1979).
[27] D.J. Adams, "Calculating the low temperature vapour line by Monte Carlo", *Mol. Phys.*, **32**, 647 (1976).
[28] L.A. Rowley, D. Nicholson and N.G. Parsonage, "Long-range corrections to grand canonical ensemble Monte Carlo calculations for adsorption systems", *J. Comp. Phys.*, **26**, 66 (1978).
[29] W.A. Steele, *The Interaction of Gases with Solid Surfaces*, Pergamon, New York, (1974).
[30] G.C. Maitland, M. Rigby, E.B. Smith and W.A. Wakeham, *Intermolecular Forces: their origin and determination*, Oxford University Press, (1981).
[31] M.R. Reddy and S.F. O'Shea, "The equation of state of the two-dimensional Lennard-Jones fluid", *Can. J. Phys.*, **64**, 677 (1986).
[32] L. Medros, E. Chacón, G. Navascués and M. Lombardero, "Two-dimensional Lennard-Jones liquid-vapour interphase. A functional perturbation approach", *Mol. Phys.*, **54**, 211 (1985).
[33] R. Evans and P. Tarazona, "Wetting and thick-thin film transitions in a model of argon at a solid CO_2 substrate", *Phys. Rev. A*, **28**, 1864 (1983).
[34] B.C Freasier and S. Nordholm, "The generalized van der Waals theory of wetting; non-local entropy and oscillatory structures", *Mol. Phys.*, **54**, 33 (1985).
[35] P. Tarazona and R. Evans, "Wetting transitions at models of a solid gas interface", *Mol. Phys.*, **48**, 799 (1983).
[36] D.J. Adams, "Chemical potential of hard-sphere fluids by Monte Carlo", *Mol. Phys.*, **28**, 1241 (1974).
[37] D.J. Adams, "Grand canonical ensemble Monte Carlo for a Lennard-Jones fluid", *Mol. Phys.*, **29**, 307 (1975).
[38] D. Nicholson and N.G. Parsonage, *Computer Simulation and the Statistical Mechanics of Adsorption*, Academic Press, London, 1982.
[39] M.H. Mezei, "Grand-canonical ensemble Monte Carlo study of dense liquid. Lennard-Jones, soft spheres and water", *Mol. Phys.*, **61**, 565 (1987)
[40] A. Munster, *Statistical Thermodynamics*, Vol 1, Springer, Berlin, 1969.
[41] J. R Henderson and F. van Swol, "On the interface between a fluid and a planar wall. Theory and simulations of a hard sphere fluid at a hard wall", *Mol. Phys.*, **51**, 991 (1984).
[42] P. Schofield and J.R. Henderson, "Statistical mechanics of inomogeneous fluids", *Proc. R. Soc. A*, **379**, 231 (1982).
[43] J.P.R.B. Walton, D.J. Tildesley and J.S. Rowlinson, "The pressure tensor at the planar surface of a liquid", *Mol. Phys.*, **48**, 1357, (1983).
[44] J.R. Henderson and J.S. Rowlinson,"Statistical mechanics of fluid interfaces in cylindrical symmetry", *J. Phys. Chem.*, **88**, 6484 (1984).
[45] M. Schoen, D.J. Diestler and J.H. Cushman, "Fluids in micropores. I. Structure of a simple classical fluid in a slit-pore", *J. Chem. Phys.*, **87**, 5464 (1987).

[46] W. van Megen and I.K. Snook. "Physical adsorption of gases at high pressure I. The critical region", *Mol. Phys.*, **45,** 629 (1982).
[47] I.K. Snook and W. van Megen, "Physical adsorption of gases at high pressure II. Effect of temperature", *Mol. Phys.*, **47,** 1417 (1982).
[48] J.P.R.B. Walton and T.P.J. Halpin, "A simple molecular graphics program", in preparation (1988).
[49] CHEMGRAF, created by E.K. Davies, Chemical Crystallography Laboratory, Oxford University, developed and distributed by Chemical Design Ltd, Oxford.
[50] T.L. Hill, "Statistical mechanics of multimolecular adsorption. III. Introductory treatment of horizontal interactions. Capillary condensation and hysteresis", *J. Chem. Phys.*, **15,** 767 (1947).
[51] G. Mason, "A model of adsorption-desorption hysteresis in which hysteresis is primarily developed by the interconnections in a network of pores", *Proc. R. Soc. A*, **390,** 47 (1983).
[52] D. Nicholson, Presentation at CCP5 workshop on *Sorption in Porous Solids*, Imperial College, London, July (1987).
[53] G.A. Chapela, G. Saville, S.M. Thompson and J.S. Rowlinson, "Computer simulation of a gas-liquid surface. Part 1. ", *J. Chem. Soc. Faraday Trans. II*, **73,** 1133, (1977).
[54] N.A. Seaton, J.P.R.B. Walton and N Quirke, work in progress (1988).